PREPARED FOR THE U.S. DEPARTMENT OF ENERGY,
UNDER CONTRACT DE-AC02-76-CHO-3073

PPPL-2835
UC-426,427

PPPL-2835

A MICROSPHERE-BASED SHORT-WAVELENGTH RECOMBINATION X-RAY LASER

BY

E.J. VALEO AND S.C. COWLEY

April, 1992

PPPL PRINCETON PLASMA PHYSICS LABORATORY

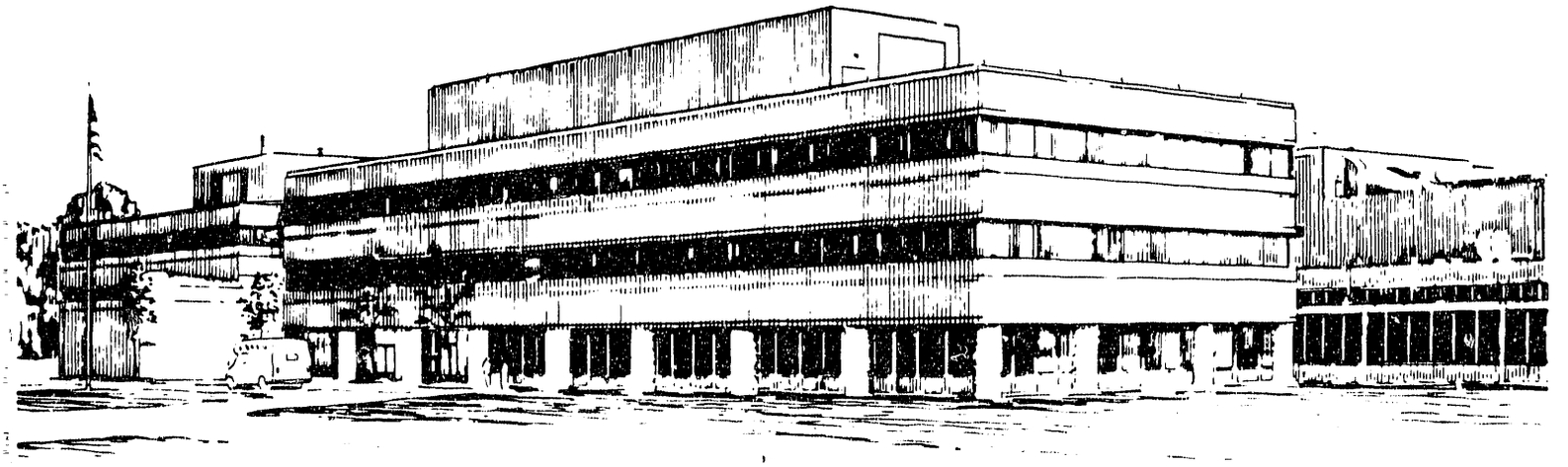

PRINCETON UNIVERSITY, PRINCETON, NEW JERSEY

NOTICE

NOTICE

PPPL--2835

DE92 013244

A Microsphere-Based Short-Wavelength Recombination X-Ray Laser

E.J. Valeo and S.C. Cowley
Princeton Plasma Physics Laboratory
P.O. Box 451, Princeton, New Jersey 08543

Abstract

We describe a scheme for obtaining very short wavelengths ($\lambda \sim 10\mathring{A}$) in recombination lasers. The rapid cooling rates necessary to achieve population inversion during recombination are attained by adiabatic expansion of sub micron spheres. The lasing region is made up of many such spheres. The spheres are heated impulsively by a powerful picosecond laser. First, they ionize, then as they expand, they cool and recombine. We have calculated the optimum sphere size and initial temperature for maximum gain in the $n = 3$ to $n = 2$ transition of hydrogen-like ions of elements with atomic numbers, Z, between 10 and 30. Gain of about $10^3\,\mathrm{cm}^{-1}$ is calculated in aluminum at $38.8\mathring{A}$. Gain rapidly decreases with Z so that gain in titanium at $13.6\mathring{A}$ is about $40\,\mathrm{cm}^{-1}$. We have calculated the required pump laser intensity and found it to be attainable with current lasers. The propagation of the pump through the "gas" of spheres is considered and the problems arising from pump scattering by the spheres are discussed.

I. Introduction

X-Ray laser development is proceeding at a rapid rate. Since the demonstration of lasing action at X-ray wavelengths in 1984[1–3] there has been steady progress in many areas, including achievement of increased gain-length products and progression to shorter wavelengths. The future holds the promise of widespread application of these systems to areas as diverse as microlithography, microscopy and holography.[4]

We propose here a novel method of achieving recombination-pumped gain at lasing wavelengths of order $10\mathring{A}$. The laser is similar to other recombination-pumped devices that operate successfully at longer wavelengths, in so far as a high temperature plasma is created by irradiation of a target medium with a so-called pump laser. Subsequently, the nonequilibrium conditions required for lasing are achieved by cooling the plasma sufficiently rapidly to reach a "superionized" state – one in which the ionization stage exceeds that achievable under steady-state conditions at the ambient density and temperature.

Production of the strongly nonequilibrium conditions required for gain in recombination-pumped X-ray lasers becomes problematic at short wavelengths. A picosecond cooling rate is desirable for lasing at wavelengths approaching $10\mathring{A}$. This rate can be achieved with adiabatic expansion of sub-micron sized targets. The rate cannot be achieved with radiative cooling in a single-species plasma. The fastest adiabatic cooling rate is achieved in a spherical expansion (three dimensional expansions cool faster than two or one dimensional expansions). There are, in fact, three main reasons why we expect small spherical targets to be optimal. First, as we have said, they have the highest adiabatic cooling rates and therefore the highest gains. Second, small spheres have a large surface area to volume ratio and thus require less pump laser intensity to heat. Third, sub-micron spheres are relatively easy to fabricate compared to, for instance, sub-micron fibers.

In Section II we calculate gain in expanding isothermal spheres. The isothermal assumption is justified by the short thermal conduction time. A simple similarity model of the hydrodynamic expansion and collisional radiative model of the atomic physics are used. The initial temperature, T_0, the initial radius, R_0, and the atomic number, Z, of the sphere are inputs to our calculation. We calculate the gain, g_{32}, in the $n = 3$ to $n = 2$ transition of the hydrogen-like ion. By varying T_0 and R_0, we find the optimum values

for maximum gain. The maximum of g_{32} for a given element, Z, is plotted in Figure 7. The pump laser must heat the sphere to the initial temperature in a fraction of the expansion time–*i.e.* in a fraction of a picosecond. The required pump laser intensity is calculated to be attainable with currently available sub-picosecond lasers (see Figure 10).

While spherical targets provide an ideal cooling geometry, they don't, of course, provide an ideal lasing geometry. The lasing region should be long enough to provide a gain length product of perhaps ten. It must also be narrow enough to be optically thin to the "dump" transition for the lower lasing level which, in our case, is the $n = 2$ to $n = 1$ transition. In aluminum these requirements yield the optimum lasing region to be about 100 microns long and 2 microns wide. This geometry can be accomplished with multiple sub-micron targets, "microspheres," suspended in a vacuum or low density gaseous medium. Perhaps the simplest method of suspending the spheres is to give them sufficient kinetic energy that their pressure supports them against gravity. The "gas" of microspheres is arranged to have a mean mass density equal to the mean mass density of a single microsphere at the time of peak gain. Clearly the optimum size of the microspheres and their spacing can be obtained from the single sphere calculations. The microsphere gas is placed in the focus of the pump laser. The focal region defines the lasing geometry, see Figure 1. The pump laser will propagate in the microsphere gas with some scattering and absorption. At high Z the scattering makes the simple pumping scheme of Figure 1 inappropriate (see Section III E). Other pumping geometries are therefore suggested for high Z. Thus, with the appropriate pump intensity, spheres in the focal region are heated to the optimum temperature for gain. The heated spheres expand and fill the space, forming a relatively uniform high gain region. Our design raises the possibility of efficient generation of sho r wavelengths than are currently available.

In Section II, we consider the evolution of a single sphere of initial temperature T_0 and radius R_0. The hydrodynamic similarity model of the expansion is discussed in Section II A. In Section II B, we present a simple model of the atomic physics to aid understanding. The full computational model is presented in Section II C. In Section III, we discuss the heating by the pump laser and the propagation of the pump laser in the microsphere gas. The isothermal assumption is justified in Section III A. The absorption and scat-

tering of the pump laser by the spheres is calculated in Section III B. In Section III C, we calculate the required pump intensity. The physical constraints on the size and shape of the lasing region are calculated in Section III D. Finally we calculate the propagation of the pump laser in Section III E. In the conclusion we discuss future work and other applications of the microsphere "gas".

II. Gain in a Single Sphere

In this section we consider the evolution of a single sphere and the gain achieved in the evolution. We shall calculate the optimum values of the initial sphere radius R_0 and initial temperature T_0 for maximum gain. The gain, g_{32}, in the $n = 3$ to $n = 2$ transition in hydrogen-like ions is calculated. In Section A we consider the hydrodynamic evolution of a sphere (which fortunately decouples from the atomic physics). A simple analytic calculation of the atomic physics is presented in Section B. This calculation is not quantitatively accurate but it does show the scaling trends and it does aid our understanding. Results from the model are summarized in Figure 3. There we plot the maximum value of g_{32} the values of T_0 and R_0 which maximize gain, all as a function of Z. In Section C we present the computational model and our results, which are displayed in Figures 5-8.

A. Hydrodynamic evolution of Microsphere

The objective is to heat the sphere of radius R_0 to a uniform temperature T_0 – which for now we specify only as being comparable to the ionization potential of that ion stage which will subsequently lase – in a time short compared to the disassembly time C_S/R_0. We shall be dealing with fully stripped ions and hydrogen-like ions with atomic numbers, Z, greater than 10. The initial sound speed, C_S, is therefore given by $C_S = (ZT_0/2M)^{1/2}$ where M is the mass of the ion. The electron density in a solid ($\sim 10^{24}\,\mathrm{cm}^{-3}$) greatly exceeds the critical density, where the laser freqmency ω equals the local electron plasma frequency ω_{pe}, for currently available lasers of the required intensity and pulse duration ($n_{cr} \sim 10^{21} - 10^{22}\,\mathrm{cm}^{-3}$). Additionally, although the optimal sphere radius can be substantially smaller than the wavelength of the pump laser, it typically greatly exceeds the collisionless

skin depth c/ω_{pe}. Therefore, the pump laser deposits energy at the surface of the sphere. The pump intensity required to deposit this energy is considered in Section III C. If the sphere is too large, the time for thermal diffusion from the heated surface to the center will exceed the disassembly time, with the result that the core will remain cold and relatively weakly ionized. In Section III A we show that the isothermal assumption holds for the spheres we consider. Cold matter will absorb the X-rays by bound-free transitions.[5] It is therefore desirable to keep the lasing medium relatively isothermal. The atoms are ionized to the hydrogen-like stages very rapidly. In modeling the hydrodynamic expansion we make use of the large value of Z. The change in electron density due to the ionization from the hydrogen-like state is neglected since it produces a relative density change of order Z^{-1}. We also neglect the energy involved in ionization, recombination and atomic transitions, since it is typically a fraction Z^{-1} of the energy in free electrons. These approximations allow us to decouple the hydrodynamic problem from the atomic physics. If the plasma is allowed to freely expand into vacuum, then, after it increases its dimensions to a size substantially larger than R_0, its further evolution will be well described by a similarity solution of the hydrodynamic equations.[7] Within this model, to a good approximation, the current plasma size $R(t)$, density $n(t) \equiv n(r = 0, t)$ and temperature $T(t)$ are determined in terms of their corresponding initial values R_0, n_0, and T_0 by the simple relations:

$$\frac{d^2R(t)}{dt^2} = \left(\frac{C_S}{R(t)}\right)^2 \quad , \tag{1a}$$

$$T(t) = T_0 \cdot \left(\frac{R_0}{R(t)}\right)^{\lambda_T} \quad , \tag{1b}$$

$$n(t) = n_0 \cdot \left(\frac{R_0}{R(t)}\right)^{\lambda_n} \quad , \tag{1c}$$

and where λ_T, (resp. λ_n) takes on the value $2d/3$, (resp. d) with $d = 1, 2, 3$ in the case of planar, cylindrical and spherical geometry, respectively. From Eq. (1a), we see that for $R(t) >> R_0$, we have the simple result $R(t) \simeq R_0 C_S t$. Eq. (1b) follows from the conservation of entropy in adiabatic expansion and Eq. (1c) follows from the conservation of particles.

Having obtained the density evolution at the symmetry point $r = 0$, the

off-axis density follows from the similarity form

$$n(r,t) = n(t)\exp\Big\{-\frac{1}{2}\Big[\frac{r}{R(t)}\Big]^2\Big\} \quad , \tag{2}$$

B. Analytic Model

In this section we will examine a simple analytic model of the atomic physics in an expanding sphere. (The quantitative results of this section differ from our more detailed numerical results but the qualitative features are correct.) Let us consider the origin of the sphere only and let us take the long time approximation to $R(t)$, i.e., $R(t) \simeq R_0 + C_S t$. We normalize Z to ten (since we are interested in Z between ten and thirty), T_0 to the ionization potential for the hydrogen-like ion, R to R_0, R_0 to 10^{-5} cm and the initial density, n_0 to 10^{24} cm^{-3}. Thus $Z = 10\bar{Z}$, $T_0(\text{eV}) = 1360\bar{Z}^2\bar{T}_0$, $x = R/R_0$, $R_0(\text{cm}) = 10^{-5}\bar{R}_0$, and $n_0(\text{cm}^{-3}) = 10^{24}\bar{n}_0$. We also take the atomic mass number to be $2Z$. The lasing wavelength in these units is $\lambda_{32}(\mathring{A}) = 65.6/\bar{Z}^2$. In normalized units the expansion rate is,

$$\frac{dx}{dt} = \frac{C_{S0}}{R_0} = 2.6\cdot 10^{12}\frac{\bar{Z}\sqrt{\bar{T}_0}}{\bar{R}_0}\ \text{sec}^{-1} \quad . \tag{3}$$

During the early stages of the expansion we require ionization to dominate so that a population of fully stripped ions is obtained. The initial electron temperature must therefore be comparable to the ionization potential of the hydrogen-like ion (i.e. $\bar{T}_0 \sim O(1)$). At this temperature ionization to the hydrogen-like state is very rapid. We shall therefore assume (both for the analytic and numerical work) that initially all atoms are in the ground state of the hydrogen-like ion.

Our simplified model for the hydrogen-like ion is illustrated in Figure 2. The model consists of three levels in the hydrogen-like ion and the fully stripped ion. The $n = 1$ ground state has the fractional population n_1, the $n = 2$ and $n = 3$ excited levels have fractional populations n_2 and n_3 respectively and the fully stripped ion has a fractional population n_∞. Clearly, $n_1 + n_2 + n_3 + n_\infty = 1$.

The fractional populations of the excited states, n_2 and n_3, are typically much smaller than the fractional populations in the ground state n_1 and fully

stripped state n_∞. This is just a result of the fact that the collisional sources for these levels are typically smaller than the radiative decay rates. The analytic model contains the following transition rates between levels $n = 1$, $n = 2$, and $n = 3$: The collisional excitation rate between $n = 1$ and $n = 2$, denoted C_{12}, the radiative transition rate between $n = 3$ and $n = 2$ (A_{32}), the radiative transition rate between $n = 2$ and $n = 1$ (A_{21}) and the collisional deexcitation rate between $n = 3$ and $n = 2$ (C_{32}). The collisional excitation from level $n = 2$ is ignored as $n_2 << 1$ and the collisional deexcitation rate from $n = 2$ is unimportant compared to the radiative decay. We consider single step ionization from the $n = 1$ level only. Ionization from $n = 2$ and $n = 3$ is small when the radiative rates dominate and n_2, n_3 are populated less than the thermal equilibrium value. At the densities of interest ($n \sim 10^{22} - 10^{24}\,\mathrm{cm}^{-3}$) three body recombination dominates radiative recombination. The electrons preferentially recombine into the upper levels of the atom. The upper levels are approximately in Boltzmann / Saha equlibrium as the collisional transition rates are high. The lower levels, however, are dominated by radiative decay. One develops a picture of a recombining electron diffusing (random walking) through the upper levels of the atom until it reaches some critical lower level. At this critical level n_c radiative decay dominates and the electron rapidly decays to the ground state. Obviously no population inversion can occur in levels above n_c because they are in Saha equlibrium. The diffusional flux of electrons through the upper levels has been calculated by many authors (see Zeldovich,[15] Pert.[14]) to be proportional to $Z^3 n^2 / T^{9/2}$. In our normalized units this yields the recombination rate due to this process,

$$R_\infty = 1.3 \cdot 10^{11} \frac{\bar{n}_0^2}{\bar{T}_0^{9/2} \bar{Z}^6} x^3 \ \mathrm{sec}^{-1} \quad , \tag{4}$$

where we have used Eqs. (1b) and (1c) for $T(x)$ and $n(x)$. We assume R_∞ gives the net recombination rate and that a fraction b of this rate gives the flux of electrons from $n > 3$ levels into the $n = 3$ level. Thus we have modeled the effect of the levels with $n > 3$ on the source for level $n = 3$. Note direct recombination into the $n = 3$ level without passing through the higher n states is relatively unimportant.

We will assume that the initial electron temperature is smaller than the $n = 2$ to $n = 1$ transition energy. The collisional rates $C_{1\infty}$ and C_{12} can be

calculated using the cross sections for ionization and excitation at threshold. These cross sections are independent of energy and proportional to Z^{-4}. The rates $C_{1\infty}$ and C_{12} are obtained by averaging σv over the maxwellian (for more complete approximations see Keane's thesis[16]). Thus in normalized units

$$C_{1\infty} \simeq 20.6 \cdot 10^{12} \frac{\bar{n}_0}{\bar{Z}_0^3 \sqrt{\bar{T}_0}} \frac{1}{x^2} \exp\left(-\frac{x^2}{\bar{T}_0}\right) \text{ sec}^{-1} \quad , \tag{5}$$

$$C_{12} \simeq 30 \cdot 10^{12} \frac{\bar{n}_0}{\bar{Z}_0^3 \sqrt{\bar{T}_0}} \frac{1}{x^2} \exp\left(-\frac{3}{4}\frac{x^2}{\bar{T}_0}\right) \text{ sec}^{-1} \quad , \tag{6}$$

The $n = 3$ to $n = 2$ collisional deexcitation, C_{32}, is obtained from C_{23} by detailed balance. Thus we find

$$C_{32} \simeq 25 \cdot 10^{12} \frac{\bar{n}_0}{\bar{Z}_0^3 \sqrt{\bar{T}_0}} \frac{1}{x^2} \text{ sec}^{-1} \quad . \tag{7}$$

The mean radiative rates[17] are

$$A_{21} = 4.7 \cdot 10^{12} \bar{Z}^4 \text{ sec}^{-1} \quad , \tag{8}$$

$$A_{32} = 0.43 \cdot 10^{12} \bar{Z}^4 \text{ sec}^{-1} \quad , \tag{9}$$

and

$$A_{31} = .55 \cdot 10^{12} \bar{Z}^4 \text{ sec}^{-1} \quad . \tag{10}$$

For values of $\bar{Z}$ of interest ($\bar{Z} \sim 1.5$) the radiative rates A_{21}, A_{32} and A_{31} are larger than the expansion rate and the ionization and recombination rates. The populations of the $n = 3$ and $n = 2$ levels are therefore in quasi-steady state, i.e.,

$$n_3 \simeq b n_\infty \frac{R_\infty}{(A_{32} + A_{31} + C_{32})} \quad , \tag{11}$$

$$n_2 \simeq \frac{1}{A_{21}} (A_{32} n_3 + C_{12} n_1) \, . \tag{12}$$

The ionization recombination balance in the model is

$$\frac{dn_1}{dt} = R_\infty n_\infty - C_{1\infty} n_1 \, . \tag{13}$$

Since n_2, $n_3 << n_1$, n_∞, we set $n_\infty = 1 - n_1$ and we use Eq. (3) to replace $d/dt = (dx/dt)d/dx$. Thus,

$$\frac{dn_\infty}{dx} = -0.05\frac{\bar{R}_0\bar{n}_0^2}{\bar{T}_0^5\bar{Z}^7}x^3 n_\infty + 8\frac{\bar{n}_0\bar{R}_0}{\bar{T}_0\bar{Z}^4}\frac{1}{x^2}\exp\left(-\frac{x^2}{\bar{T}_0}\right)(1-n_\infty)\,. \qquad (14)$$

Typically we shall be interested in situations where $\bar{T}_0 \sim O(1)$ (although we have assumed $\bar{T}_0 < 1$ to derive $C_{1\infty}$ and C_{12}) and $\bar{R}_0 \sim O(1)$. Clearly ionization dominates Eq. (14) at $x = 1$. As the sphere expands (x increases) the ionization rate drops rapidly and the recombination rate rises rapidly. Thus the evolution splits rather naturally into two phases – the ionization phase and the recombination phase. The total fractional ionization after the ionization phase, n_∞^1, can be estimated by ignoring recombination over this time. Thus

$$n_\infty^1 \simeq 1 - \exp(-\alpha) \quad , \qquad (15)$$

where

$$\alpha = 8\frac{\bar{n}_0}{\bar{T}_0}\frac{\bar{R}_0}{\bar{Z}^4}\int_1^\infty \frac{1}{x^2}\exp\left(-\frac{x^2}{\bar{T}_0}\right) \sim 4\frac{\bar{n}_0\bar{R}_0}{\bar{Z}^4}\exp -\frac{1}{\bar{T}_0} \quad , \qquad (16)$$

and we have evaluated α in the limit $\bar{T}_0 < 1$. Physically α represents the amount of ionization in the first expansion time. When $\bar{R}_0$ or $\bar{T}_0$ is small the sphere expands and cools before significant ionization occurs. During the recombination phase typically when $x >> \bar{T}_0$ we may ignore ionization in Eq. (14) and obtain,

$$n_\infty \sim n_\infty^1 \exp -\beta\frac{x^4}{4} \quad ,$$

where

$$\beta = 0.05\frac{\bar{R}_0\bar{n}_0^2}{\bar{T}_0^5\bar{Z}^7} \quad , \qquad (17)$$

is roughly the amount of recombination in the first expansion time.

There is, in fact, a third phase in the evolution where ionization and recombination balance and the left hand side of Eq. (14) is negligible (the quasi-static situtation). This occurs for parameters of interest when $\beta x^4 >> 1$ and n_∞ is small. In the quasi-static phase

$$n_\infty \sim \frac{H(x)}{1+H(x)} \quad , \qquad (18)$$

where

$$H(x) = 160\frac{\bar{T}_0^4}{\bar{n}_0}\bar{Z}^3\frac{1}{x^5}\exp(-\frac{x^2}{\bar{T}_0}) \quad .$$

As we shall see, gain occurs during the recombination phase and not during this later steady state phase. If $\beta \geq 1$ ($\bar{T}_0 << 1$ or $\bar{R}_0 >> 1$) then the recombination phase does not exist – the initial ionization phase takes the ion directly into the quasi-static phase.

The gain per unit length, g_{ul}, for a transition from level u to level l is

$$g_{ul} = Gn_e\frac{\lambda_{ul}^4}{\Delta\lambda}A_{ul}\left[n_u - n_l\frac{g_u}{g_l}\right] \tag{19}$$

where

$$G = \frac{1}{8\pi c}\left(\frac{1}{2\pi}\right)^{1/2} \quad , \tag{20}$$

and the linewidth

$$\Delta\lambda = \lambda\frac{C_S}{c} \quad , \tag{21}$$

is due to the doppler width caused by the expansion of the spheres.[8,9] In our case, the degeneracies $g_j = j^2$. Using Eqs. (11) and (12) and the rates, Eqs. (4) – (10) we obtain,

$$g_{32} \sim 1.6\cdot 10^6\frac{\bar{n}_0}{\bar{Z}^8\bar{T}_0^{1/2}x^3}\Big\{\frac{\bar{n}_0^2 bx^3}{\bar{T}_0^{9/2}\bar{Z}^6}\frac{n_\infty}{Q_u} - \frac{85\bar{n}_0}{\bar{Z}^3\bar{T}_0^{1/2}}\frac{1}{x^2}\exp\left(-\frac{3}{4}\frac{x^2}{\bar{T}_0}\right)(1-n_\infty)\Big\} \quad . \tag{22}$$

The first term in the braces is essentially proportional to the recombination rate, where the factor

$$Q_u \equiv (1 + \frac{60\bar{n}_0}{\bar{Z}^7\bar{T}_0^{1/2}}\frac{1}{x^2}) \quad , \tag{23}$$

is the "quenching coefficient", defined as the ratio of the total deexcitation rate (collisional pus radiative) to the radiative decay rate of the upper lasing level. The second term in Eq. (22) is the excitation from $n = 1$ to $n = 2$ populating the $n = 2$ level and lowering the gain. For large $\bar{T}_0$ and small x the second term dominates and the gain is negative. Since g_{32} is a monotonically

increasing function of n_∞ and x it must increase during the ionization phase when n_∞ and x are increasing. Substituting Eq. (18) into Eq. (22) we see that the gain is always negative in the quasi-static phase.

We have calculated (numerically) the maximum value of g_{32} from Eq. (22), maximising with respect to x, T_0 and R_0. In Figure 3 we plot the maximum g_{32} as a function of Z, together with the values of R_0 and T_0 which optimize g_{32}. In these computations, we estimate b by

$$b_{br} = \frac{A_{43} + C_{43}}{(A_{43} + C_{43} + A_{42} + A_{41})} \quad .$$

which is the branching ratio into level 3 from level 4. The maximum g_{32} given by this model exceeds the numerical result of Section II C by a factor of ten for $Z = 20$. However, since the model is rather simplified, numerical accuracy is not expected.

A number of qualitative features can be understood from this model. First let us consider the steep inverse scaling of g_{32} with Z. At high Z the collisional rates are small and therefore $n_3 \sim [R_\infty/(A_{32} + A_{31})]n_\infty$. Using $n_i \propto Z^{-1}$, $\Delta\lambda \propto \lambda Z$, $\lambda \propto Z^{-2}$ and $R_\infty \propto Z^{-6}$ and setting $n_2 \sim 0$ and $n_\infty \sim 1$ we obtain from Eq. (22) $g_{32} \propto Z^{-14}$. At low Z collisional deexcitation dominates the decay from the $n = 3$ level ($Q_a >> 1$), thus $n_3 \sim (R_\infty/C_{32})n_\infty$ and $g_{32} \sim Z^{-7}$. Note we have implicitly assumed that $\bar{T}_0$ and n_∞ do not scale significantly with Z; their calculated scalings are indeed mild. Clearly the dominant reasons for the strong decrease in gain with increasing Z are the scalings of R_∞ and λ.

The existence of a maximum g_{32} can be understood, again qualitatively, from our model. First consider the initial temperature, $\bar{T}_0$. If $\bar{T}_0$ is small the amount of ionization and therefore gain is small. Conversely if $\bar{T}_0$ is large the recombination rate is always small, the $n = 1$ to $n = 2$ excitation rate is large and the gain is consequently small. Clearly an optimal temperature exists. Now consider the initial radius, $\bar{R}_0$. If $\bar{R}_0$ is small the sphere expands very rapidly and cools before significant ionization takes place. However if $\bar{R}_0$ is large the cooling is slow and the atom is in a quasi-equilibrium where $n = 1$ to $n = 2$ excitation populates the $n = 2$ level and shuts off the gain. Again we expect an optimum $\bar{R}_0$. These opposing tendencies are sketched in Figure 4.

The advantages of spherical expansion are also apparent from our model.

Clearly we hope to achieve significant initial ionization but insignificant ionization during the recombination phase. Thus one wishes to have an ionization rate and an $n = 1$ to $n = 2$ excitation rate that decrease rapidly with x and a recombination rate that increases rapidly with x. Now consider three types of symmetrical expansion, planar ($d = 1$), cylindrical ($d = 2$) and spherical ($d = 3$). The $n = 1$ to $n = 2$ excitation rate is proportional to $x^{-2d/3}\exp(-3x^{2d/3}/4\bar{T}_0)$ and therefore it decreases most rapidly with x when $d = 3$, *i.e.*, in spherical expansion. The ionization rate behaves similarly. The recombination rate is proportional to x^d and therefore increases most rapidly (with x) when $d = 3$. Thus spherical expansion is preferable.

C. Numerical Model

After a discussion of the numerical method, we examine in some detail the time evolution of a single sphere. This is followed by a discussion of the optimization of gain with respect to initial radius R_0 and temperature T_0, given Z. Finally, the variation of optimized gain and other critical quantitites, such as the optical depth of the dump transition, with Z are presented.

1. Numerical Method

In the general case, the evolution of the atomic states and radiation fields must be kept on a par with that of the hydrodynamic variables. Fortunately, for our system the power density associated with atomic excitation and ionization is small compared to the cooling power resulting from expansion. As we stated in Section II A, this is a consequence of the large Z. This circumstance allows an accurate computation of the evolution in two independent steps. First, the hydrodynamic evolution is computed neglecting the power flow into internal atomic states. Then the density and temperature so computed enter as time dependent parameters in the computation of the atomic state.

Given the time evolution of the fluid variables, the evolution of the fractional populations of the ground and excited states of the hydrogen-like ion, and of the fully-stripped ion are computed in a Lagrangian frame

$$\frac{d\mathbf{r}}{dt} = \mathbf{V} \quad , \tag{24}$$

with $\mathbf{V}(\mathbf{r}(t), t)$, the local flow velocity. We neglect ionization from and recombination to lower ionization stages on the grounds that during the heating phase, collisional ionization from He-like ions will occur on a much shorter time scale whenever significant gain is achieved, and that during the recombination phase, recombination into He-like ions will not affect the gain calculations. With these remarks, the governing equations for the bound state fractional populations are

$$\frac{dn_j}{dt} = S_j + C_j - I_j + R_j \quad . \tag{25}$$

Here

$$S_j = \Sigma_{j'>j} A_{j'j} n_{j'} - \Sigma_{j'<j} A_{jj'} n_j \quad , \tag{26}$$

is the net spontaneous transition rate into level j, expressed in terms of the individual rates $A_{j'j}$ from j' to j,

$$C_j = n_e[\Sigma_{j' \neq j}(C_{j'j} n_{j'} - C_{jj'} n_j)] \quad , \tag{27}$$

is the net rate of collisional excitation into level j from expressed in terms of the rate coefficient $C_{jj'}$ from j to j',

$$I_j = n_e n_j C_{j\infty} \quad , \tag{28}$$

is the ionization rate from level j, expressed in terms of the ionization rate coefficient $C_{j\infty}$, and

$$R_j = n_e n_s (n_e \alpha_{tb,j} + \alpha_{rad,j}) \quad , \tag{29}$$

is the sum of the three-body and radiative recombination rates ($\alpha_{tb,j}$ and $\alpha_{rad,j}$, respectively) into level j. All sums over bound states are up to a level l which is varied to check convergence. The rate coefficents are those given by Keane.[16]

The equation for the evolution of the fractional population of fully stripped ions is

$$\frac{dn_\infty}{dt} = I_\infty - R_\infty \quad , \tag{30}$$

where

$$I_\infty = \Sigma_j I_j \quad , \tag{31}$$

is the total rate of collisional ionization from, and

$$R_\infty = \Sigma_j R_j \quad , \tag{32}$$

is the sum of recombination rates into, all bound states. By virtue of the relations Eqs. (31), (32) and the additional evident relation

$$\Sigma_j C_j = 0 \quad , \tag{33}$$

we have that the total population

$$n_t \equiv \Sigma_j n_j + n_\infty \quad , \tag{34}$$

is onserved,

$$\frac{dn_t}{dt} = 0 \quad . \tag{35}$$

By definition $n_t = 1$.

There is a large variation in the magnitude of the rate coefficients in the set of equations (25) and (30), both with changes in temperature and in quantum number. This variation could be expected to cause difficulty in a numerical solution, but the set has been found to be amenable to accurate solution with standard scientific library algorithms.[18] The chosen algorithm conserves density to machine roundoff (10^{-15}).

Once the fractional populations are computed, the gain at line center for the 3 to 2 transition follows immediately from Eqs. (19) - (21).

2. Time Evolution

As an illustrative example, we present results for the time evolution of a Titanium sphere ($Z = 22$) in Figure 5a-e. The initial radius of the sphere $R_0 = 2.17 \cdot 10^{-5}\,\mathrm{cm}$. It is assumed initially at rest $\dot{R}(t = 0) = 0$. The electron density on axis, $n(t) \equiv n_e(r = 0, t)$ is initially set to $1 \cdot 10^{24}\,\mathrm{cm}^{-3}$, essentially solid density. The sphere is assumed impulsively heated to an electron temperature $T_0 = 3.1 \cdot 10^3\,\mathrm{eV}$, equal to .47 of the ionization potential of the hydrogen-like ion. The sphere is then assumed to freely expand into vacuum. The evolution of the sphere size $R(t)$ is obtained by solving Eq. (1a). $T(t)$ and $n(t)$ are then obtained by evaluation of Eqs. (1b) and (1c), respectively. All three are plotted in Figure 5a. We note there the decrease of $T(t)$ by more than a factor of 9 in 1.5 psec.

Given the hydrodynamic evolution, the state populations are then computed as described in Section II C 1. We have found that inclusion of seven excited states, with principal quantum numbers $n = 2, \ldots, 8$, adequately describes the hydrogen-like system for these purposes. This was confirmed in two ways: First sensitivity of computed gain to changes was shown to be small. Second, during the interesting time interval, the populations of all but the first 4 or so levels were seen to be quite close to Saha quilibirium (*ie.*, within $\sim 5\%$) with the free electron - fully stripped ion populations. The evolution of the fractional population of the ground state of the hydrogen-like ion, n_1 and of the line-center gain at $r = 0$, g_{32} are presented in Figure 5b. Ionization proceeds to a level of 12% in 320 fsec, followed by recombination with an effective rate of about $1.2 \cdot 10^{12}\,\mathrm{sec}^{-1}$. Upon onset of recombination, the gain rises rapidly to $38.3\,\mathrm{cm}^{-1}$ at 860 fsec and then decays at a rate comparable to the fully-stripped population. Several characteristic features of these profiles persists through our scans in R_0, T_0 and Z. First, the width of the gain profile is comparable to the delay in its onset after impulsive heating. This has the important consequence that, in practice, producing overlap amongst the gain profiles of an ensemble of similar spheres is readily achievable. Second, especially at higher Z's (say above 15) the optimal maximum fractional ionization of the hydrogen-like ion is much less than unity (as was assumed in the analysis of Section II B) . We find that for such Z values, if ionization fractions of order unity are achieved, then recombination induced gain is much less than optimal.

The fractional populations of the upper and lower lasing levels,n_3, resp., n_2, are shown in Figure 5c. Again, consistent with the assumptions of the collisional-radiative model,[12] and with the neglect of effects of doubly-excited states, fractional excitations are small.

Further diagnostics are presented in Figure 5d. There the line-center optical depth for the dump transisiton, defined here as $\tau_{12} \equiv g_{12}(r = 0, t) \cdot R(t)$, although several initially is seen to drop to .87 at peak gain. Similarly, the quenching coefficient at $r = 0$,

$$Q(t) \equiv \frac{1}{A_{32}}[n_e(0,t)C_{32} + A_{32}] \quad , \tag{36}$$

drops to .46 at peak gain. Another potential gain spoiler, excitation of level 2 from the ground state is plotted there as well. The relative excitation

coefficient represented by

$$R_{ex} \equiv \frac{n_2 A_{21}}{n_1 C_{12}} \quad , \tag{37}$$

is seen to drop to .11 at peak gain.

We remark that separate computations of gain off-axis ($r \neq 0$) show that, typically, regions of positive gain extend out to radii several times $R(t)$ during the time interval of appreciable gain on axis ($r = 0$). This observation indicates that the total gain per sphere, $G(t) = 2\int_0^\infty g(r,t)\,dr$, is expected to be positive when the gain at $r = 0$ is. Additionally, we have found that G is well-represented (to factors of order unity) by $g(r = 0,\ t) \cdot R(t)$.

3. Optimization

Wit..in our model the evolution is completely characterized by the parameters R_0, T_0, and Z. Optimization of peak gain with respect to (R_0, T_0) for a given Z and determination sensitivity of the gain profile to deviations from optimum conditions have been carried out by computing on-axis evolution for a set of initial condition (R_0, T_0). As an example, the results for Titanium are shown in Figure 6. A single maximum in the peak gain of $38.3\,\mathrm{cm}^{-1}$ is achieved for $2.17 \cdot 10^{-5}\,\mathrm{cm}$, $3.1 \cdot 10^3\,\mathrm{eV}$. As predicted by the analytic model, we observe the competition between insufficient ionization for low initial temperatures and/or radii, and insufficiently rapid recombination at large initial temperatures and/or radii.

4. Variation with Atomic Number

The optimization computations of the previous section have been repreated For each Z in the range ($Z = 10$, $\lambda_{32} = 65.6\mathring{A}$) to ($Z = 30$, $\lambda_{32} = 7.29\mathring{A}$) The results are presented in Figure 7a-d. In all cases, the initial electron density was taken to be $10^{24}\,\mathrm{cm}^{-3}$. Note that since gain scales like the initial density cubed we have not considered spheres of lower initial density. Figures 8a-d give various important quantities at the time t^* of peak gain for each Z.

III. Heating and Pump laser Propagation

In this section we consider the requirments for a pump laser. In Subsection A we show that the typical thermal conduction time is short and that the isothermal assumption is good. We obtain the scattering and absorption cross sections for the spheres in Subsection B. The pump laser intensity requirements are calculated, and shown to be attainble with existing lasers in Subsection C. The "dump transition" from level $n = 2$ to $n = 1$ must be optically thin (we assumed that it was so in Section II) otherwise the population of the $n = 2$ level is large and the gain is negative. In Subsection D we discuss how this requirement limits the width of the lasing medium. Finally in Subsection E we discuss the pump propagation in the "gas" of microspheres and show that scattering of the pump light is problematic. We offer specific ideas how to minimize scattering or tolerate scattering.

A. The isothermal assumption

In this section we use the nondimensional units of Section II. We make estimates of the collisional transport of heat assuming that the sphere does not move (expand) in the times of interest. This assumption is of course justified by the fact that the calculated thermal equilibration time is short compared to the expansion time C_{S0}/R_0. The electron collision rate in inverse seconds is $\nu_e = 2.3 \cdot 10^{15} \bar{n}_0 \bar{T}_0^{-3/2} \bar{Z}^{-2}$. Therefore electrons establish a local maxwellian in a small fraction of the expansion time ($C_{S0}/R_0 = 2.6 \cdot 10^{12} \bar{Z} \bar{T}_0^{1/2} \bar{R}_0^{-1}$). Furthermore, the electron mean free path λ_{mfp} is short compared to the radius of the sphere, specifically

$$\frac{\lambda_{mfp}}{R_0} \sim 9 \cdot 10^{-2} \frac{\bar{T}_0^2 \bar{Z}^3}{\bar{n}_0 \bar{R}_0} \quad , \tag{38}$$

Thus we estimate the time to reach a uniform temperature by using the collisional transport coefficients of Braginski.[20] In order to include some geometrical factors we choose the estimated rate to be the decay rate of the lowest order (slowest decaying) eigenmode of the linearised heat diffusion equation, ν_{iso}. Thus normalising this rate to C_{S0}/R_0 we obtain,

$$\frac{\nu_{iso} R_0}{C_{S0}} \sim 110 \frac{\bar{Z}^3 \bar{T}_0^2}{\bar{R}_0 \bar{n}_0} \quad . \tag{39}$$

Our estimate uses the final temperature to estimate thermal conduction and thus slightly overestimates the heat conduction. Since heat is deposited in the collisionless skin depth, which is short compared to the sphere radius, we expect initial temperature gradients to be large and nonlocal heat conductivity to be important. However since we have a large ratio in Eq. (39) such details are not expected to change the basic conclusion that the sphere is isothermal.

B. Pump scattering and absorption from the microspheres

We shall take a simple linear electron response to the field inside the microsphere (we treat the microsphere as a dense plasma sphere). So the current **J** is given by

$$\frac{4\pi}{c}\mathbf{J} = \frac{\omega_{pe}^2 \mathbf{E}}{c(\nu_e - i\omega)} \quad , \tag{40}$$

where $\omega_{pe} = (4\pi n_{e0} e^2/m_e)^{1/2} = 5.6 \cdot 10^{16}\, \bar{n}_0^{1/2}\, \mathrm{sec}^{-1}$ is the plasma frequency, ω is the pump laser frequency and ν_e the electron collision rate. Since $\nu_e = 2.3 \cdot 10^{15}\, \bar{n}_0 \bar{T}_0^{-3/2} \bar{Z}^{-2}\, \mathrm{sec}^{-1}$ and ω is typically $7.5 \cdot 10^{15}\, \mathrm{sec}^{-1}$ for a KrF picosecond laser, $\omega_{pe} >> \omega,\ \nu_e$. we can therefore ignore the displacement current in Maxwell's equations and obtain,

$$\nabla^2 B = \frac{\omega_{pe}^2}{c^2}\Big(\frac{\omega}{\omega + i\nu}\Big)\,\mathbf{B} \quad . \tag{41}$$

Thus the **B** field and therefore the current is confined to a layer of width l_p, the skin depth,

$$l_p = \frac{c}{\omega_{pe}}\Big|\Big(\frac{\omega}{\omega + i\nu}\Big)\Big|^{1/2} \quad , \tag{42}$$

Typically for $\omega \sim \nu$, $l_p \sim 4 \cdot 10^{-7}\, \bar{n}_0^{1/2} << R_0$ and one can consider the laser heating to be in a narrow shell on the outside of the microsphere. We therefore take the limit $l_p/R_0 << 1$ and $k l_p << 1$ where $k = \omega/c$ but we shall consider $kR_0 \simeq \mathcal{O}(1)$. In this limit the sphere scatters light like a perfectly conducting sphere. The absorption is small in the parameter kl_p, and results from the deviation from the perfectly conducting approximation.

The calculation is standard, see for instance Jackson.[21] Thus the scattering cross section, σ_{sc} is,

$$\sigma_{sc}(x) = 2\pi R_0^2 \sum_{l=1}^{\infty}(2l+1)\frac{1}{x^2}\Big\{\frac{j_l^2}{j_l^2+y_l^2} + \frac{[(l+1)j_{l-1}-lj_{l+1}]^2}{[(l+1)j_{l-1}-lj_{l+1}]^2+[(l+1)y_{l-1}-ly_{l+1}]^2}\Big\} \quad ,$$

$$= \pi R_0^2 F(x) \quad , \tag{43}$$

where $x = kR_0$ and $j_l(x)$ and $y_l(x)$ are the spherical Bessel functions.[22] The absorption cross section, σ_{abs} is,

$$\sigma_{abs}(x) = \alpha(\omega)\, 2\pi R_0^2 \sum_{l=1}^{\infty}(2l+1)\frac{1}{x^4}\Big\{\frac{1}{j_l^2+y_l^2} + \frac{1}{[(l+1)j_{l-1}-lj_{l+1}]^2+[(l+1)y_{l-1}-ly_{l+1}]^2}\Big\}$$

$$= \alpha\pi R_0^2 G(x) \quad , \tag{44}$$

where

$$\alpha(\omega) = \Re\Big[\frac{-\omega}{\omega_{pe}} i(1+\frac{i\nu}{\omega})^{1/2}\Big] \quad ,$$

where $\Re$ indicates that we take the real part of the expression in the brackets. Clearly $\alpha(\omega)$ is small and the absorption cross section is small compared to the geometric cross section. We plot $F(x)$ and $G(x)$ in Figure 9. Note that for $kR_0 << 1$, $\sigma_{sc} \sim (10/3\pi)R_0^2(kr_0)^4$ (Rayleigh scattering) and $\sigma_{abs} \sim 6\pi R_0^2\,\alpha(\omega)$. Thus it is possible at long wavelength for the sacattering cross section to be smaller than the absorption cross section.

C. Intensity requirements for the pump laser

The pump laser must heat the sphere before expansion since one wants a hot high density plasma intially. Thus we shall assume that the laser pulse lasts for a time at most equal to

$$\tau_{pump} \equiv 0.5 \cdot \frac{R_0}{C_{S0}} \quad . \tag{45}$$

Using Eq. (44) for the absorption cross section we obtain the required laser intensity I, where

$$I = 2.2 \cdot 10^{16} \frac{\bar{n}_0 \bar{T}_0^{3/2} \bar{Z}^3}{\alpha(\omega) G(x)} \, \mathrm{W\,cm^{-2}}. \tag{46}$$

Note that the total energy delivered to each sphere is $\bar{Z}\bar{n}_0\bar{R}_0^3$ μJ. Typically $\nu_e << \omega$ and $\alpha \simeq \nu_e/2\omega_{pe}$. Then,

$$I \simeq 5.4 \cdot 10^{17} \frac{\bar{n}_0^{1/2} \bar{T}_0^3 \bar{Z}^5}{G(x)} \, \mathrm{W\,cm^{-2}}. \tag{47}$$

When $x = kR_0 \rightarrow 0$, $G(x) \rightarrow 6$. We see that the required intensity scales very unfarourably with $\bar{Z}$. Currently available picosecond lasers can deliver as much as $10^{19}\,\mathrm{W\,cm^{-2}}$. In Figure 10 we have plotted the required intensity of 0.25 μm light as a function of Z (using Eq. (46)) for the optimal sphere using the $R_0(Z)$ and $T_0(Z)$ obtained in Section II C. Also shown there is the corresponding maximum pump laser pulse length τ_{pump}. We note that at high Z the required intensity in fact approaches $10^{19}\,\mathrm{W\,cm^{-2}}$. One may, therefore, be forced to use a less than optimal value of T_0 at high Z. We also note that the pulse length requirement demands state of the art picosecond lasers.

D. Physics constraints on the size and shape of the lasing region

The lasing region must be long and thin so that the induced emission is emitted preferentially in the direction of elongation. The width of the lasing region is constrained to be smaller than (or of order) the optical depth of the $n = 2$ to $n = 1$ "dump" transition. The gain is spoiled if this photon is reabsorbed and electrons are excited to the $n = 2$ level. In colder material the $n = 2$ to $n = 1$ photon is absorbed in bound-free transitions. Thus, the photons are absorbed in cold spheres that surround the hot lasing medium of spheres. It is clearly desirable to have a well-delineated width (of order the $n = 2$ to $n = 1$ optical depth) to the region which is heated by the pump laser. We have calculated the $n = 2$ to $n = 1$ optical depth numerically (see Section II). In Figure 8c we plot τ_{12}^*, the number mean free paths in a

sphere radius for the dump transition photon, at the instant of peak gain, for the optimum sphere, *vs* Z. We note, from Eq. (19) that the optical depth is inversely proportional to $A_{21}\lambda_{21}^3 n_1 n_e Z^{-2} \propto Z^{-4} n_e n_1$. Since, typically, $n_1 \sim 1$, the optical depth scales like Z^4

The X-ray laser output intensity grows exponentially with the length of the lasing region, l, for l less than a critical length, l_c. Specifically, for $l < l_c$, $I \sim \exp(g_{32} l)$. When $l = l_c$ the induced decay rate from level $n = 3$ is comparable with the spontaneous or collisional decay rate. The front of the laser pulse continues to be amplified for $l > l_c$, however the response is no longer linear since the populations of the levels are affected by the laser light. The laser pulse tends to steepen and the intensity grows roughly linearly with length. At $l = l_c$ the laser intensity has the critical value I_{crit} at line center, where

$$I_{crit} \sim 2.3 \cdot 10^{11}\, \bar{Z}^4 \bar{T}^{1/2} \Big[\frac{n_3}{n_3 - g_3 n_2/g_2}\Big] \,\mathrm{W\,cm^{-2}}. \qquad (48)$$

One may also estimate that $l_c \sim 2 g_{32}^{-1} \ln(\omega/l_c)$ where ω is the width of the lasing region.

The full dynamics of the laser propagation is complicated and we shall postpone any further discussion to a future publication. We note that it might be appropriate for some applications to make multiple parallel lasing regions simultaneously – this would effectively widen the total beam diameter but still keep the width of each "beamlet" narrower than the optical depth.

E. Propagation of the pump Laser

Perhaps the simplest way to envisage heating the spheres with the picosecond pump laser is to produce a long focus and place the spheres in the focus (see Figure 1). In this scenario the spheres in the focus will be heated and the shape of the lasing region is entirely defined by the focus. As we have already stated, the width of the lasing region is constrained to be less than the optical depth of the $n = 2$ to $n = 1$ transition – this width is achievable at the focus of 0.25 μm light. Unfortunately, the scattering of light by the spheres broadens the focus and creates a problem. Let us first estimate this effect. We will consider alternatives subsequently. Let n_s be the density of spheres, R_0 the initial sphere radius and R_f the sphere radius at maximum gain. We may wish to make $n_s \sim (8R_f^3)^{-1}$ so that the space is filled by

the expansion and the gain is relatively uniform. The mean free path of the pump laser light is $\lambda_{mfp} \simeq (\sigma_{sc} n_s)^{-1}$ where the scattering cross section is given by Eq. (43). The length of the lasing region is effectively limited by λ_{mfp}. The total gain times length, g_{tot}, for a medium that is one mean free path long is

$$g_{tot} = (g_{32} R_0)\left(\frac{R_f}{R_0}\right)^3 \frac{1}{F(kR_0)} \quad , \tag{49}$$

where $F(kR_0)$ is defined in Eq. (43). Substituting numbers from our optimal cases into Eq. (49) we find $g_{tot} \simeq 50$ for $Z = 10$ ($\bar{Z} = 1$) and $g_{tot} \simeq 10^{-2}$ for $Z = 30$. Since we sould like $g_{tot} > 10$ for a moderately efficient laser we conclude that the scattering is intolerable at high Z.

There are several ways one might bypass the scattering problem – we will briefly mention two. The spheres could be placed in a narrow tube of width the optical depth. The pump laser would be focused into the tube and the scattered pump radiation would be reflected from the tube walls. The tube walls would, of course, become hot and expand but in the time scale of interest this expansion is less than the width of the tube. A second possiblity is to use a line focus and illuminate the spheres perpendicularly to the direction of gain. Achieving high intensities with a line focus may be problematic. It is also difficult to imagine producing the very sharp gradient in sphere density needed in such a scheme.

Placing the spheres in the appropriate positions may not be too hard. If one just requires a cloud of spheres one can suspend them by their thermal motions to an atmospheric scale height of approximately 50 μm. Alternatively, one may wish to drop the spheres into the path of the pump laser – on the picosecond heating timescale the spheres are stationery. Practical details such as these are really beyond the scope of this paper.

IV. Conclusions

This paper extends recombination laser schemes to shorter wavelengths. The crucial idea is to form a lasing medium from many submicron spheres. The spheres are heated by a powerful picosecond laser to temperatures comparable with the desired ionization energy. The material in a sphere is rapidly ionized and then, as the sphere expands and cools, it recombines. The desired nonequilibrium population inversion is obtained when the cooling rate

is faster than the recombination rate. This cooling time is on the of order a picosecond and the size of the spheres is chosen to achieve such cooling times. Spheres are chosen chiefly because spherical expansions produce the most rapid cooling rates. Many spheres are needed to make a significant gain length product. A schematic of one arrangement of spheres and pump laser is given in Figure 1.

We calculate the gain and other laser properties for lasing in the $n = 3$ to $n = 2$ transition in hydrogen-like ions. Ions with atomic numbers between 10 and 30 are considered. There is no reason why other lasing transitions might not be considered - we chose the simplest.

In Section II we consider the evolution of a single sphere. The expansion of the sphere is modelled (see Section II A) by an isothermal similarity model with a given initial temperature, T_0, density, n_0, and radius, R_0. A simple tractable model of the atomic physics is presented in Section II B. It is hoped that this model will aid understanding. In Section II C, we calculate the gain with a more complete numerical atomic model. The peak gain for a given Z is a function of T_0 and R_0. We calculate the optimum values of T_0 and R_0 (those values that produce the largest gain) for each Z. In Figure 7a 7b, 7c, we plot the optimum gain, R_0 and T_0 against Z. The optimum gain falls rapidly from about $10^3\,\mathrm{cm}^{-1}$ for $Z = 10$ to about $1\,\mathrm{cm}^{-1}$ when $Z = 30$.

In Section III, we consider the issues involved in heating the microspheres with a picosecond laser. The isothermal assumption is justified in Section III A. In Section III B. the absorption and scattering of the pump laser by a sphere is calculated. The required pump laser intensity is calculated in Section III C. The width of the lasing region is limited to be narrower than the optical depth of the $n = 1$ to $n = 2$ transition, as discussed in Section III D. Finally, in Section III E, we show that scattering of the pump laser beam limits the kinds of pumping schemes that are possible.

The considerations in this paper involve a number of physics processes and some of our models should be improved. In future work we intend to consider a more complete atomic model–specifically more ionization stages and more detailed calculations of the pump propagation. The experimental implementation of this idea is relatively straight forward although the pump laser requirements are at the forefront of current technology. An important consideration is the reduction of prepulse to an acceptable level. Energy in a prepulse can create a uniform warm plasma before the main pulse arrives.

This will destroy the scheme. There are many ways to reduce the prepulse and we hope to try some of them on the Princeton powerful subpicosecond laser in the future.

There are other possible uses of the microsphere "gas." For instance, coincidence pumping of one transition by another[23-25] requires the pump ion and the pumped ion to be in different plasma conditions. This could be achieved by making the spheres of the pump element a different size than the pumped element. The sizes of the spheres are chosen so that they yield the appropriate plasma conditions upon heating and expanding. The spheres are interm ngled and heated simultaneously by the pump laser. There are two advantages to this scheme. First, the geometric coupling of pump photons with pump ions would be close to 100 percent in such a scheme. Second, the plasma conditions may be controlled with some precision by controlling the sphere sizes and the pump laser intensity.

In summary, we believe that the calculations presented here indicate that lasing can be achieved at wavelengths of 10 to 40$\AA$ with our proposed scheme.

Acknowledgments

We are happy to acknowledge stimulating discussions with Russell Kulsrud, Charles Skinner, Szymon Suckewer and William Tighe. This work was supported by United States Department of Energy under Contract DE-AC02-76-CHO-3073.

References

[1]S. Suckewer, C. H. Skinner, H. Milchberg, C. Keane and D. Voorhees, Phys. Rev. Letters **55**, 1753 (1985)

[2]D. L. Mathews, *et al.*, Phys. Rev. Letters **54**, 110 (1985). (1984).

[3]M. D. Rosen, *et al.* Phys. Rev. Letters **54**, 106 (1984).

[4]S. Suckewer and C. H. Skinner, Science **247**, 1553 (1990).

[5]Assuming a bound-free absorption coefficient of order $10^{-19}\,cm^2$. See, for example, C. W. Allen, *Astrophysical Quantities*, Third Edition, Humanities Press, New Jersey (1973), page 96.

[6]C. L. S. Lewis, *et al.*, Plasma Phys. and Contr. Fusion. **30**, 35 (1988).

[7]James H. Hunter, Jr. and Ricahrd A. London, Phys. Fluids **31**, 3102 (1988).

[8]C. H. Nam, E. Valeo, S. Suckewer, and U. Feldman, J. Opt. Soc. Am. B **3**, 1199-1205 (September 1986)

[9]A. I. Shestakov and D. C. Eder, J. Quant. Spectrosc. Radiat. Transfer **42**, 483 (1989).

[10]Ya. B. Zel'dovich and Yu. P. Raizer, *Physics of Shock Waves and High-Temperature Hydrodynamic Phenomena*, Volume 1, Academic Press, New York (1966), p. 406.

[11]L. I. Gudzendo and L. A. Shelepin, Zh. Eksp. Teor. Fiz. **45**, 1445 (1963) [Sov. Phys. Jetp **18**, 998 (1964)], and Dokl. Akad. Nauk. SSSR **160**, 1296 (1965) [Sov. Phys. Dokl. **10**, 147 (1965)].

[12]R. W. P. McWhirter in *Plasma Diagnostic Techniques*, edited by R. H. Huddlestone and S. L. Leonard, Academic Press, New York (1965), chapter 5, pages 201 - 264.

[13]S. Byron, R. C. Stabler, and P. I. Bortz, Phys. Rev. Letters **8**, 376 (1962).

[14]G. J. Pert, J. Phys B, **23**, 619 (1990).

[15]Ya. B. Zel'dovich and Yu. P. Raizer, *Physics of Shock Waves and High-Temperature Hydrodynamic Phenomena*, Volume 1, Academic Press, New York (1966), p. 406.

[16]C. J. Keane, *Studies of XUV Population Inversion in CO_2 Laser Produced Plasmas*, Ph. D. Thesis, Department of Astrophysical Sciences, Princeton University (1986).

[17]Hans. A. Bethe and Edwin E. Salpeter, *Quantum Mechanics of One- and Two- Electron Atoms*, Plenum, New York (1977), page 266.

[18]*NAG Fortran Library, Mark 14*, NAG Inc, Downers Grove, IL, (1990), routine D02NBF (64 bit precision).

[19]S. Suckewer and H. Fishman, J. Appl. Physics **51**, 1922 (1980).

[20]S. I. Braginskii, "Transport Processes in a Plasma," in *Reviews of Plasma Physics*, edited by M. A. Leontovich, Vol. 1, Consultants Bureau, New York (1965), page 205.

[21]J. D. Jackson, *Classical Electrodynamics*, John Wiley & Sons, Inc., New York (1975).

[22]M. Abramowitz and I. A. Stegun, *Handbook of Mathematical Functions*, National Bureau of Standards, Applied Mathematics Series - 55, Washington, DC (1972), p. 435.

[23]B. A. Norton and N. J. Peacock, J. Phys. B **8**, 989 (1975).

[24]A. V. Vinogradov, I. I. Sobel'man, and E. A. Yukov, Sov. J. Quanmt. E.ect **5**, 59 (1975).

[25]K. J. Ilcisin, *A Study of Resonant Photopumping of Molybdenum VII for the development of a VUV Laser*, Ph. D. Thesis, Department of Astrophysical Sciences, Princeton University (1991).

[26]D. Kim, C. H. Skinner, A. Wouters, E. Valeo, D. Voorhees, and S. Suckewer, Journ. Opt. Soc. America B, **6**, 115 (1989).

[27]S. Suckewer, C. H. Skinner, D. Kim, E. Valeo and A. Wouters, Phys. Rev. Letters **57**, 1004 (1986).

[28]C. Keane and C. H. Skinner, Physical Review A **33**, 4179 (1986).

[29]G. J. Pert and S. J. Rose, Appl. Phys. B **50**, 307 (1990).

[30]B. H. Ripin, *et al.*, Phys. Rev. Letters **59**, 2299 (1987)

Figures

FIG. 1. Lasing geometry showing focal region defining elongated gain structure.

FIG. 2. Diagram of 4-level laser used in analytic investigation of gain.

FIG. 3. Variations with atomic number Z as predicted by the analytic model. *Left scale:* Maximum on-axis gain $g_{32}(\,\mathrm{cm}^{-1})$, (*solid*) optimized over both R_0 and T_0. *Right scale:* Initial sphere radius $R_0(\,\mathrm{cm})$ (*short-dash*) and initial electron temperature $T_0(\,\mathrm{eV})$ (*long-dash*) which lead to maximum gain.

FIG. 4. Sketch illustrating competing effects which lead to a maximum in gain as a function of initial sphere radius R_0 and temperature T_0 for a given atomic number Z.

FIG. 5. Time evolution of hydrodynamic and atomic variables for titanium, $Z = 22$, which has a lasing wavelength of 13.6$\mathring{A}$. The initial conditions are those which yield the largest value of the maximum in $g_{32}(t)$. The initial radius $R_0 = 2.17 \cdot 10^{-5}\,\mathrm{cm}$. The initial electron temperature $T_0 = 3.1 \cdot 10^3\,\mathrm{eV}$. In all figures, the time ranges from the instant of heating (time = 0) to 2.5 psec thereafter.

a. Evolution of hydrodynamic variables. *Left scale:* electron density $n(\,\mathrm{cm}^{-3})$ (*solid*), electron temperature $T(\,\mathrm{eV})$ (*short-dash*). *Right scale:* sphere radius, R, as defined through Eq. (??) (*long-dash*).

b. Evolution of the fractional population of the ground state, n_1, of the hydrogen-like ion (*dashed*) and of the line-center gain $g_{32}(\,\mathrm{cm}^{-1})$ at $r = 0$ (*solid*).

c. The fractional populations of the upper and lower lasing levels, n_3 (*solid*), resp., n_2 (*dashed*).

d. The line-center optical depth for the dump transisiton, defined here as $\tau_{12}(r = 0, t) \cdot R(t)$, is 3 initially, but drops to .87 at the time (.86 psec) of peak gain.

e. The quenching coefficient at $r = 0$, $Q(t)$, defined by Eq. (36), drops to .46 at peak gain. The importance of excitation of the lower lasing

level by collisional excitation from the ground state is characterized by the relative excitation coefficient R_{ex}, defined by Eq. (37), which is seen to drop to .11 at peak gain.

FIG. 6. Contour plot of peak gain *vs.* initial sphere radius R_0 and electron temperature T_0, for $Z = 22$. The maximum occurs for $R_0 = 2.17 \cdot 10^{-5}\,\mathrm{cm}$ and $T_0 = 3.1 \cdot 10^3\,\mathrm{eV}$ is for the same parameters as the evolution plots of Figure 5.

FIG. 7. Variations with atomic number Z as predicted by the numeric model.

a. Maximum on-axis gain $g_{32}(\,\mathrm{cm}^{-1})$, optimized with respect to both R_0 and T_0.

b. Initial sphere radius $R_0(\,\mathrm{cm})$ which leads to maximum gain.

c. Initial electron temperature $T_0(\,\mathrm{eV})$ which leads to maximum gain.

FIG. 8. Various quantities at the instant t^* of peak gain *vs* atomic number Z.

a. Fractional ionization, n^*_∞, (*long-dash*) upper, n^*_3, (*solid*) and lower, n^*_2, (*short-dash*) lasing level fractional populations.

b. Time, t^*, (*solid*) and relative expansion x^* (*dashed*).

c. Opacity of dump transition $\tau^*_{12} \equiv g_{12}(r = 0, t^*) * R(t^*)$.

d. Quenching, Q^*, (*solid*) and relative excitation R^*_{ex} (*dashed*).

FIG. 9. Plots of single-sphere scattering function $F(x)$, (*dashed*) Eq. (43), and absorption function $G(x)$, (*solid*) Eq. (44), *vs* normalized pump laser wavevector $x = kR$.

FIG. 10. Pump Intensity $I(\mathrm{W\,cm}^{-2})$ required to achieve maximum gain vs Z, as calculated from Eq. (46) (*solid*), together with the corresponding required maximum pump laser pulse length $\tau_{pump}(\,\mathrm{sec})$, from Eq. (45) (*dashed*).

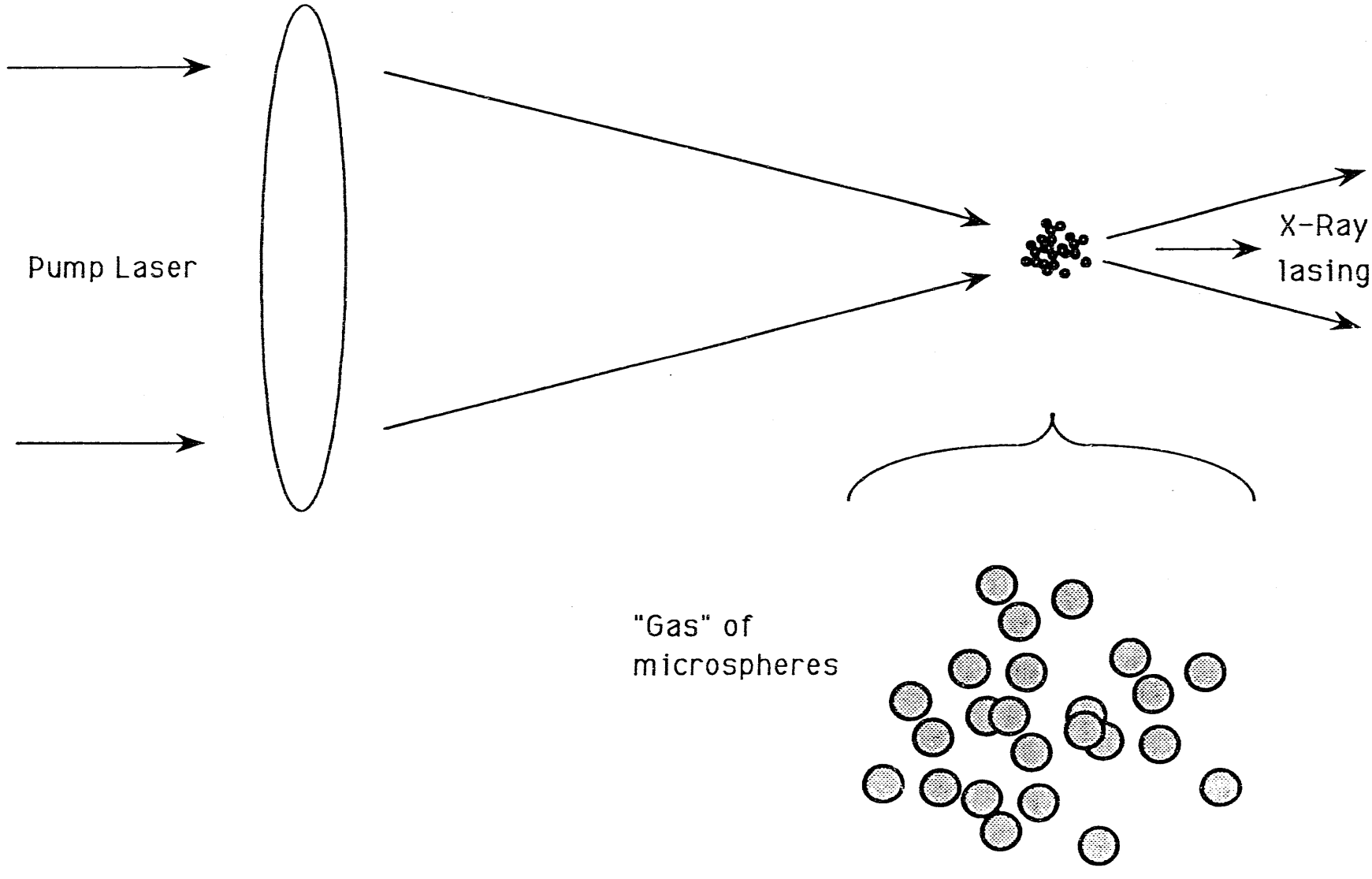

Fig. 1

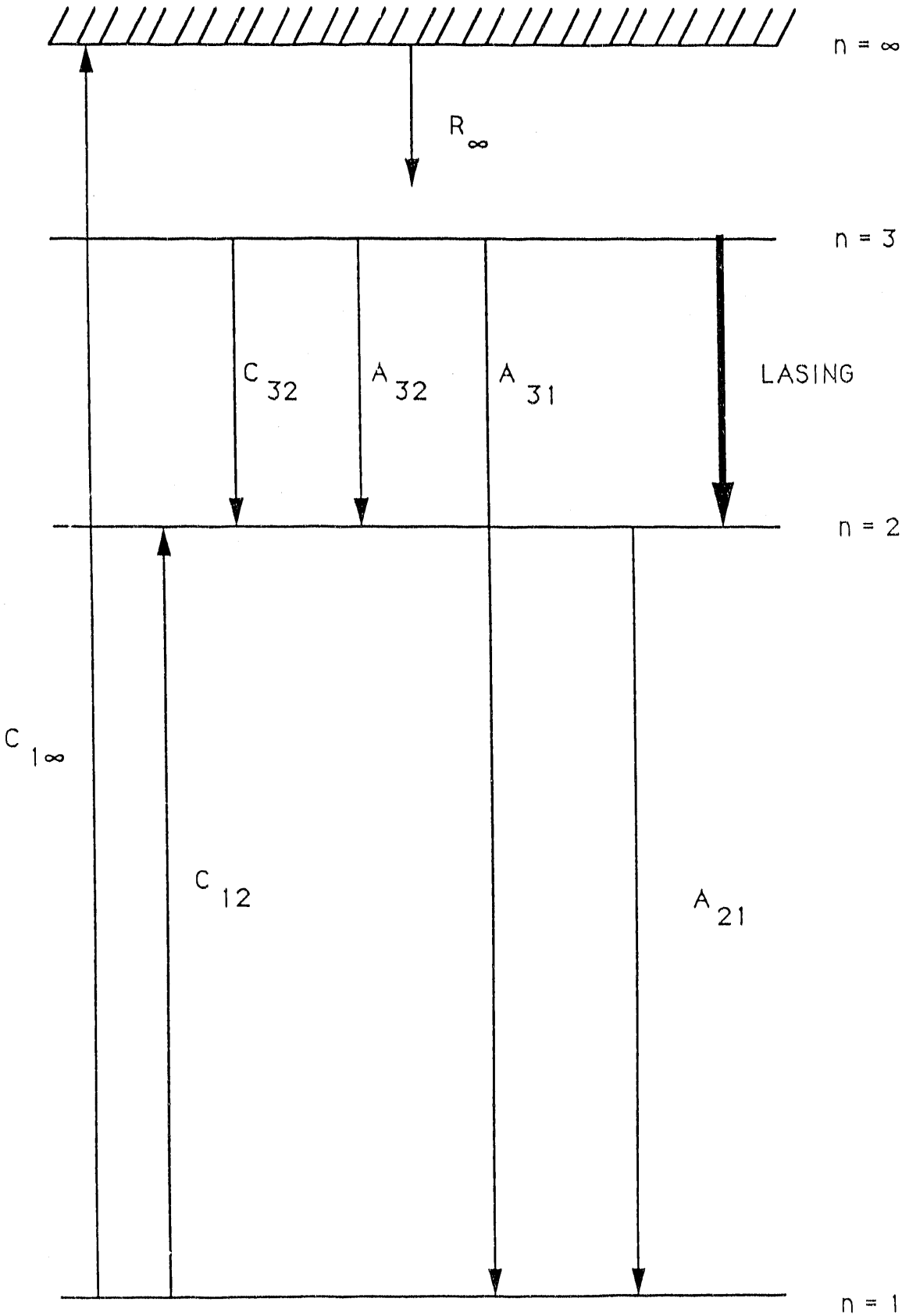

Fig. 2

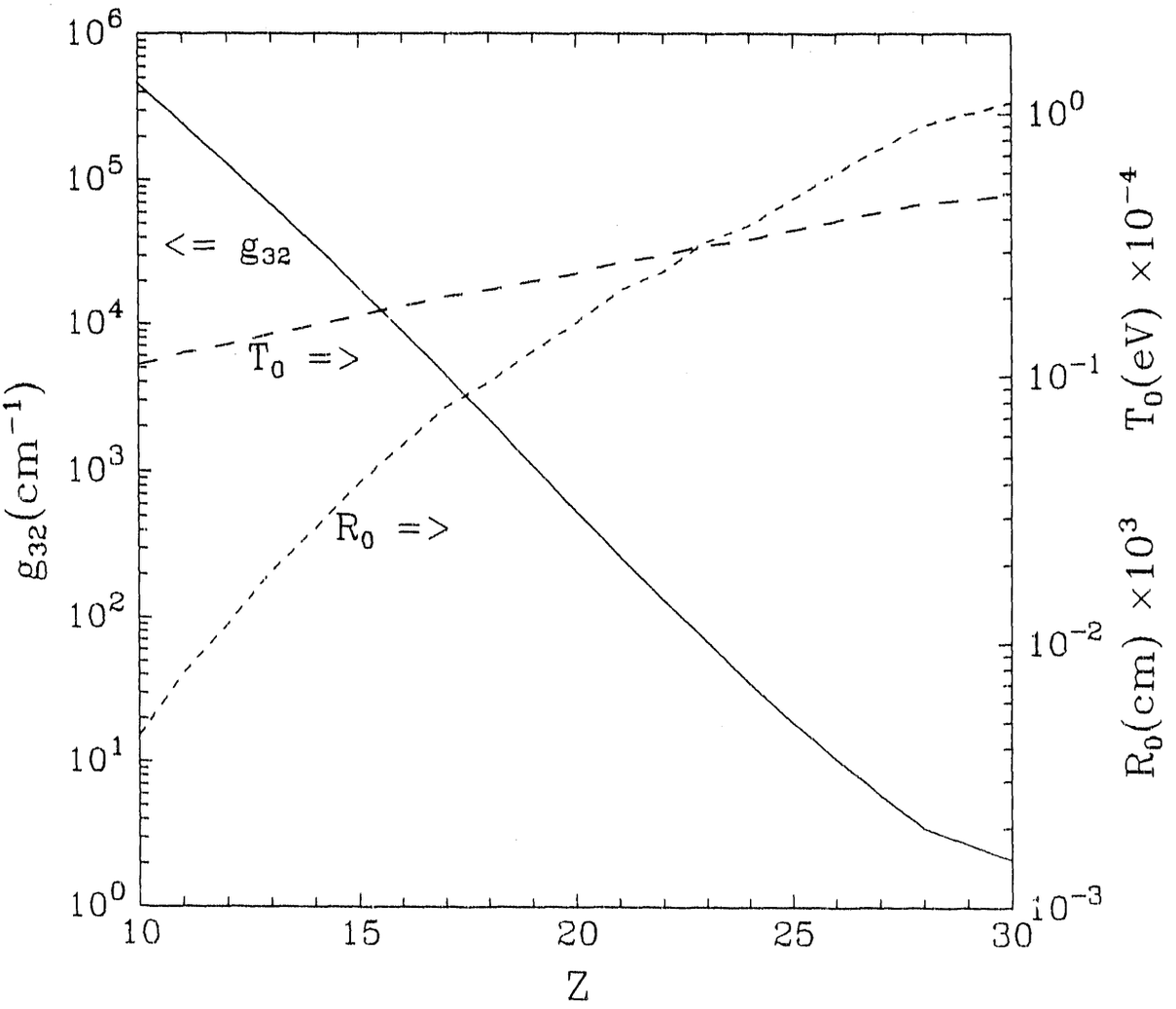
10^6
10^5
10^4
10^3
10^2
10^1
10^0
$g_{32}(cm^{-1})$
<= g_{32}
T_0 =>
R_0 =>
10
15
20
25
30
Z
10^0
10^{-1}
10^{-2}
10^{-3}
$R_0(cm) \times 10^3$
$T_0(eV) \times 10^{-4}$

Fig. 3

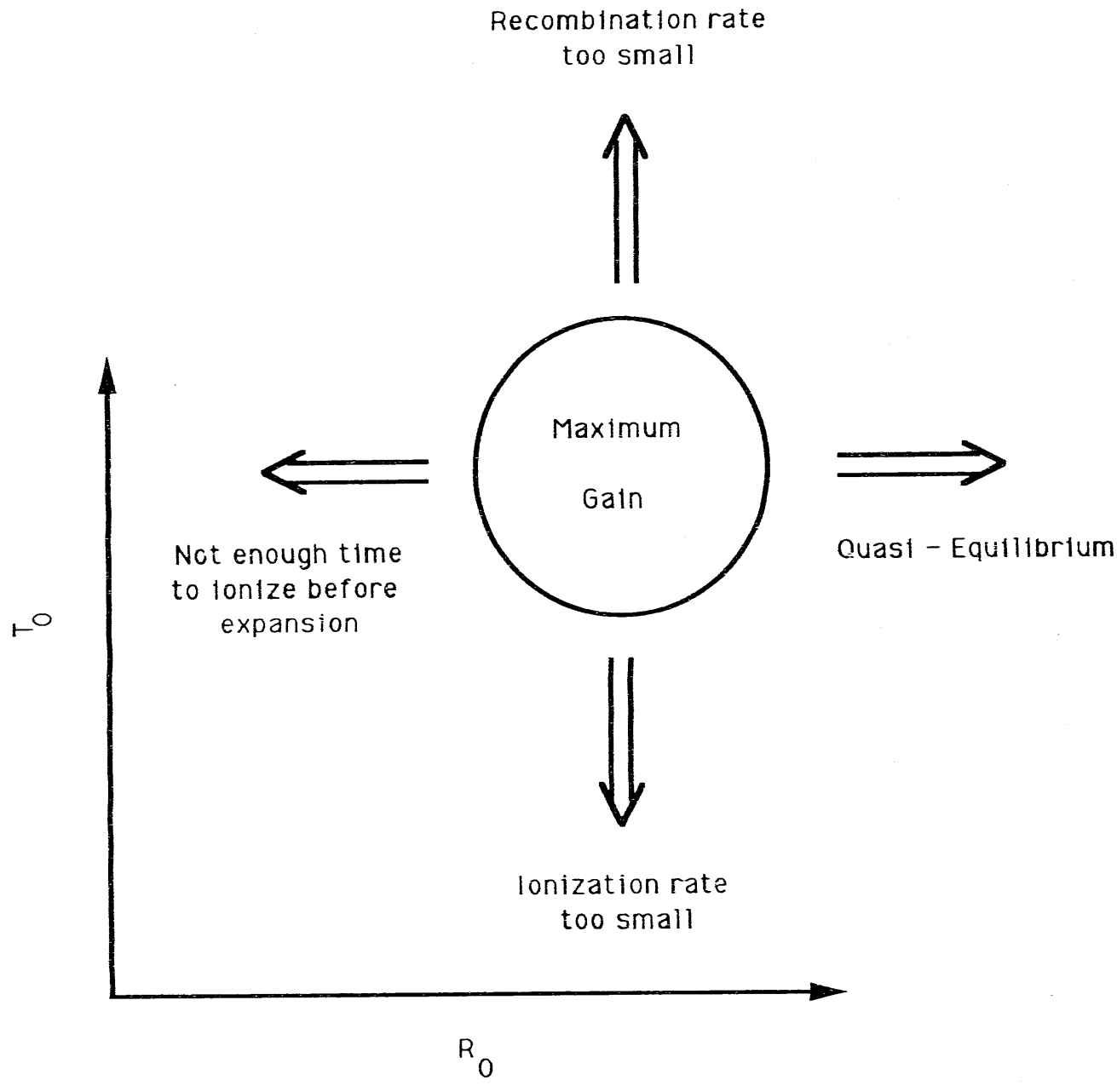
Recombination rate
too small
Maximum
Gain
Not enough time
to ionize before
expansion
Quasi - Equilibrium
Ionization rate
too small
T_0
R_0

Fig. 4

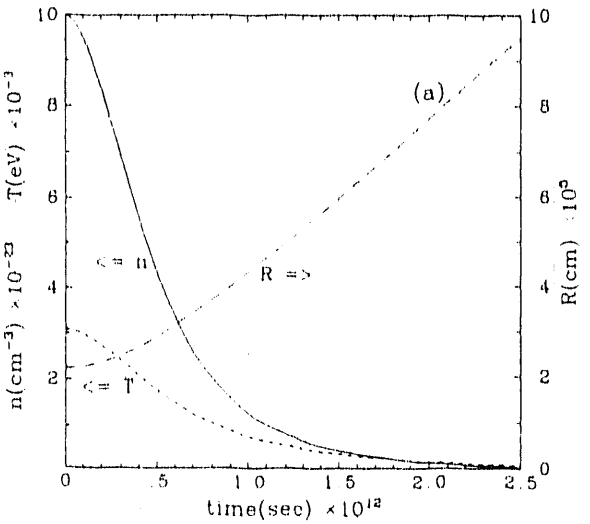
(a)
R(cm) ×10^5
time(sec) ×10^12

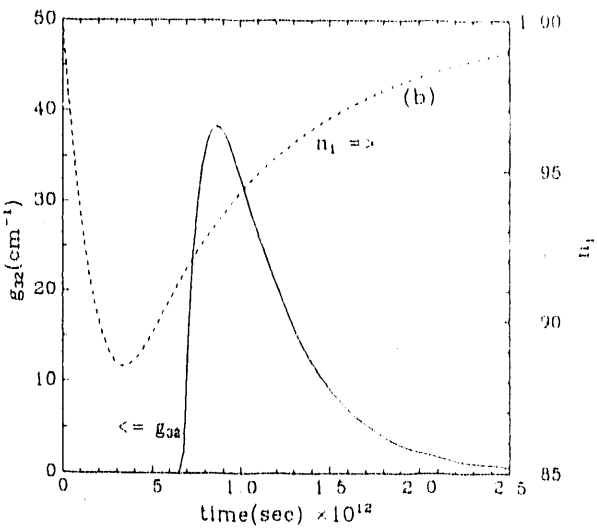
(b)
g32(cm^-1)
time(sec) ×10^12

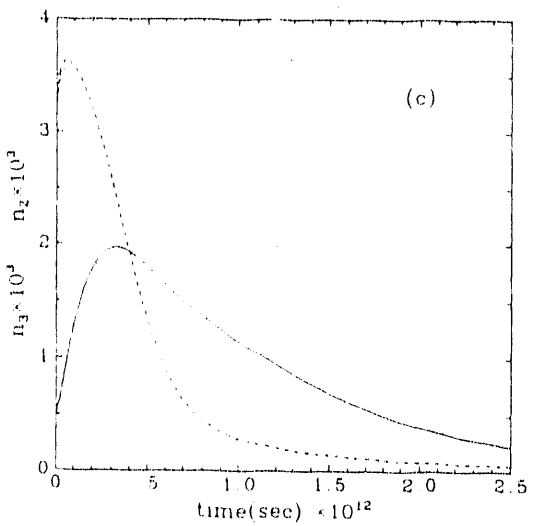
(c)
time(sec) ×10^12

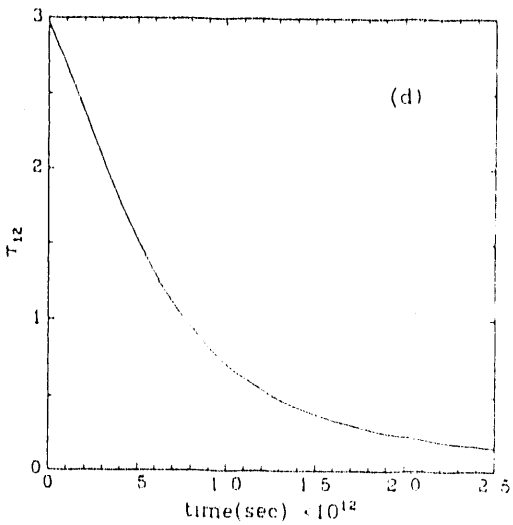
(d)
time(sec) ×10^12

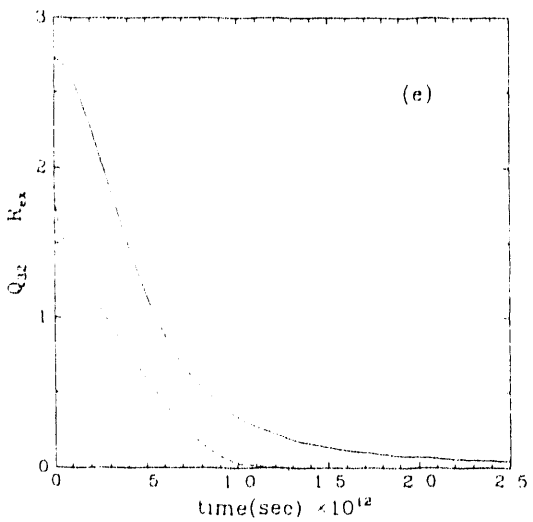
(e)
time(sec) ×10^12

Fig. 5

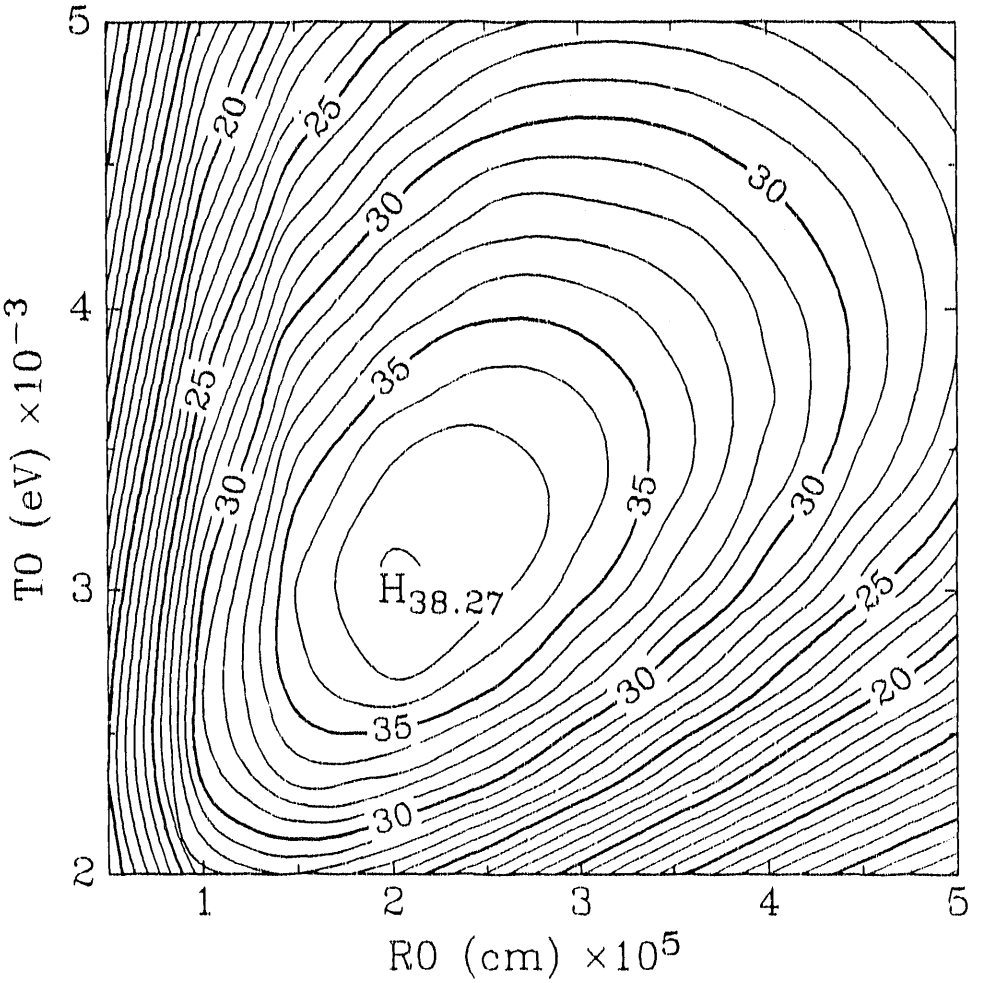

Fig. 6

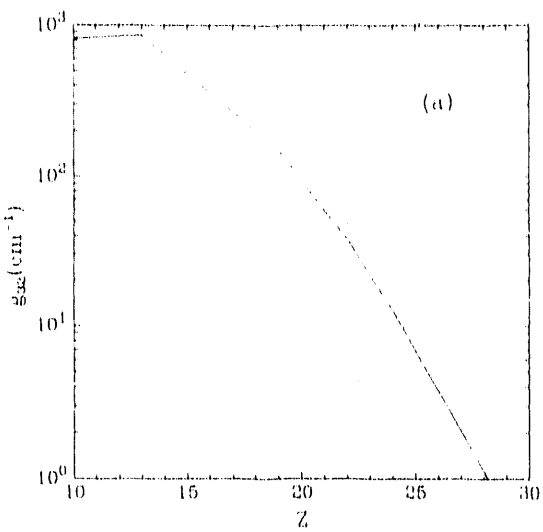
(a)
10^3
10^2
10^1
10^0
$g_{ac}(cm^{-1})$
10
15
20
25
30
Z

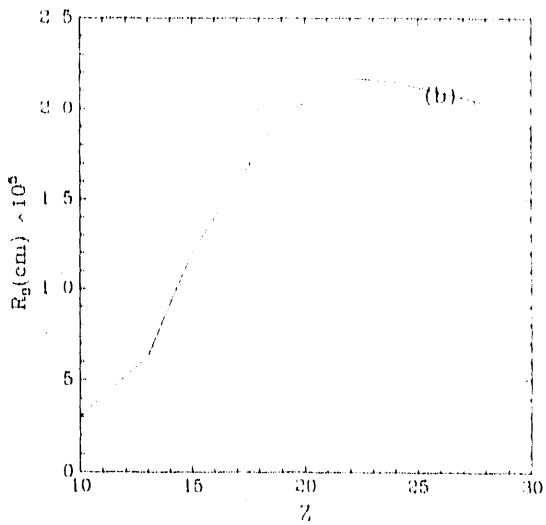
(b)
2 5
2 0
1 5
1 0
5
0
$R_g(cm) \times 10^3$
10
15
20
25
30
Z

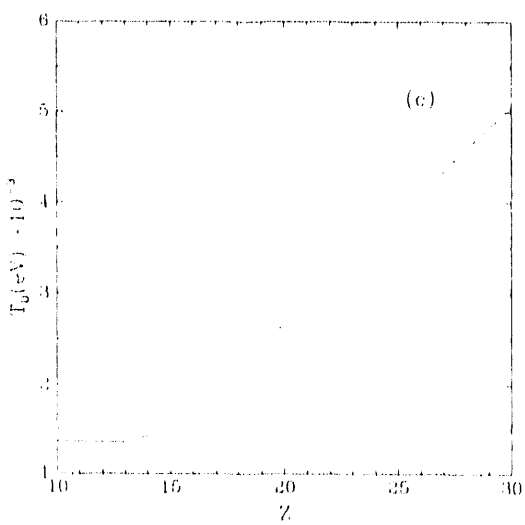
(c)
6
5
4
3
2
1
10
15
20
25
30
Z

Fig. 7

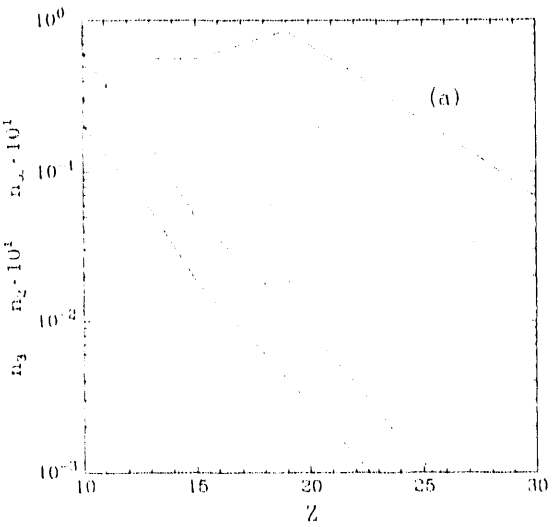

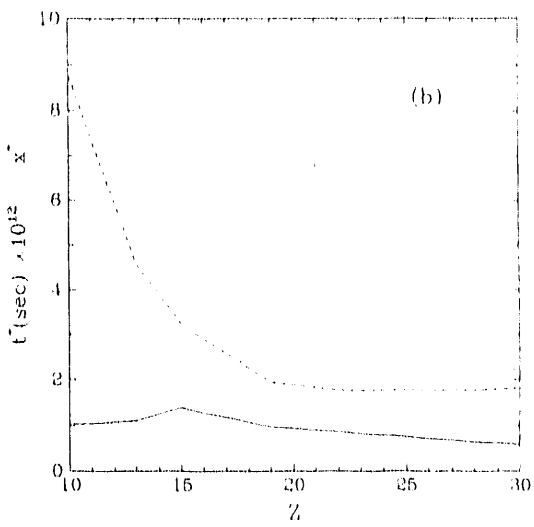

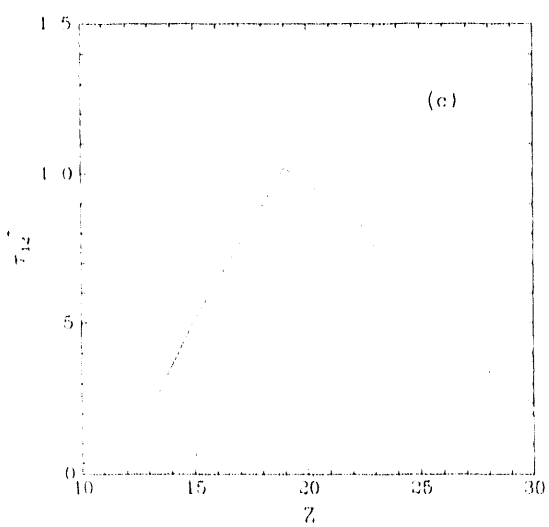

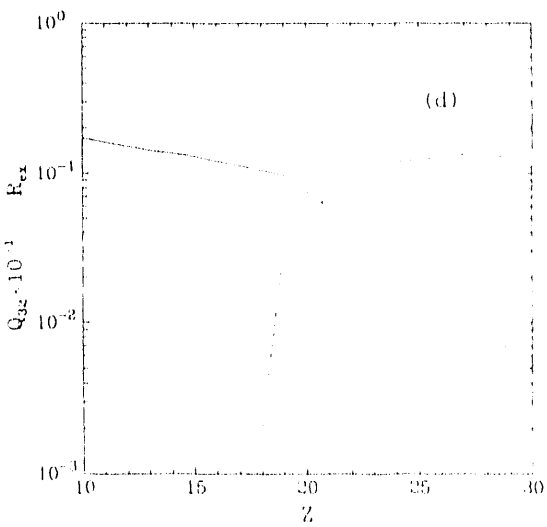

Fig. 8

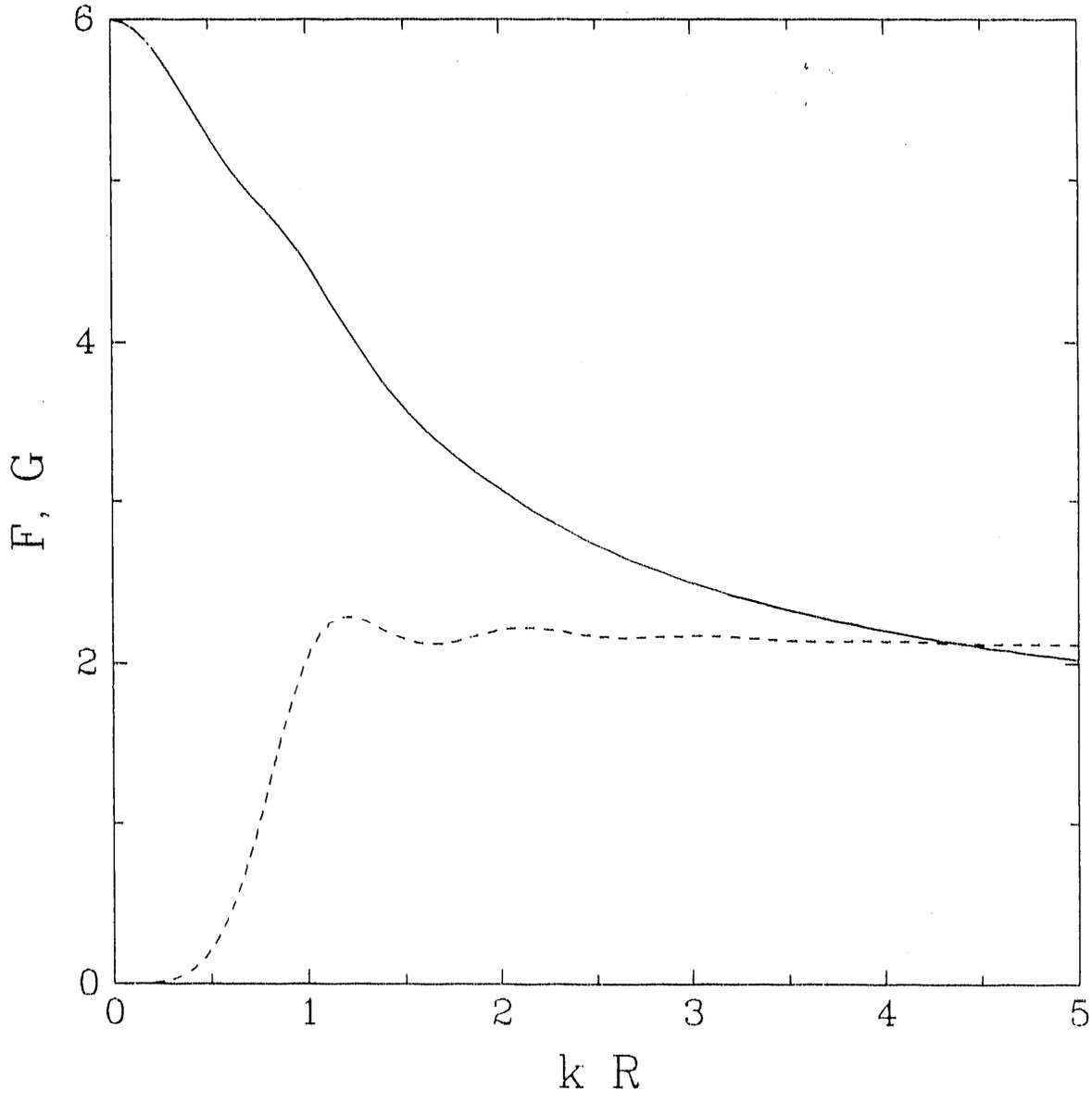

Fig. 9

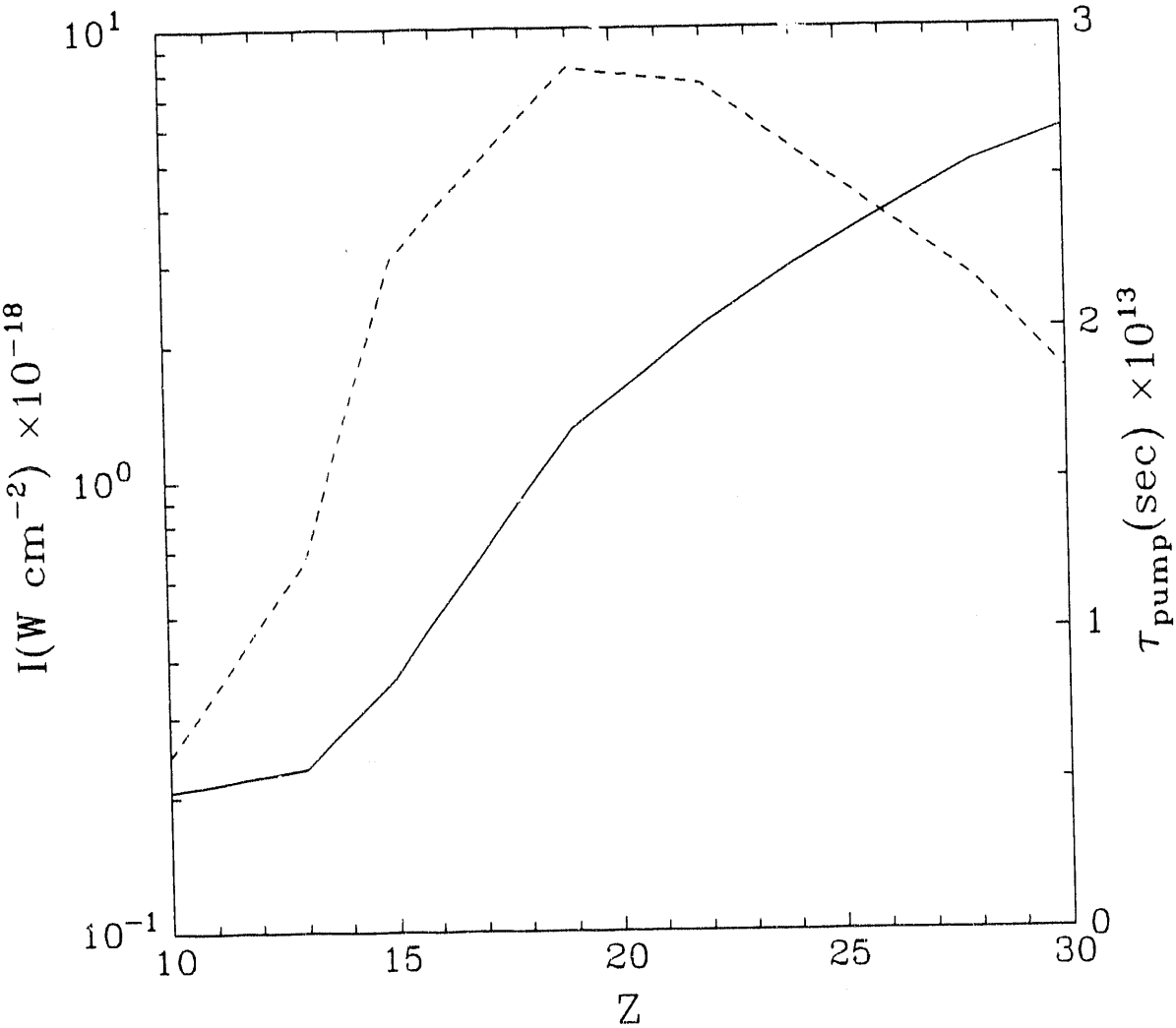
10^1
10^0
10^{-1}
$I(W\ cm^{-2}) \times 10^{-18}$
10
15
20
25
30
Z
3
2
1
0
$\tau_{pump}(sec) \times 10^{13}$

Fig. 10

EXTERNAL DISTRIBUTION IN ADDITION TO UC-420

Dr. F. Paoloni, Univ. of Wollongong, AUSTRALIA
Prof. M.H. Brennan, Univ. of Sydney, AUSTRALIA
Plasma Research Lab., Australian Nat. Univ., AUSTRALIA
Prof. I.R. Jones, Flinders Univ, AUSTRALIA
Prof. F. Cap, Inst. for Theoretical Physics, AUSTRIA
Prof. M. Heindler, Institut für Theoretische Physik, AUSTRIA
Prof. M. Goossens, Astronomisch Instituut, BELGIUM
Ecole Royale Militaire, Lab. de Phy. Plasmas, BELGIUM
Commission-European, DG. XII-Fusion Prog., BELGIUM
Prof. R. Boucique, Rijksuniversiteit Gent, BELGIUM
Dr. P.H. Sakanaka, Instituto Fisica, BRAZIL
Instituto Nacional De Pesquisas Espaciais-INPE, BRAZIL
Documents Office, Atomic Energy of Canada Ltd., CANADA
Dr. M.P. Bachynski, MPB Technologies, Inc., CANADA
Dr. H.M. Skarsgard, Univ. of Saskatchewan, CANADA
Prof. J. Teichmann, Univ. of Montreal, CANADA
Prof. S.R. Sreenivasan, Univ. of Calgary, CANADA
Prof. T.W. Johnston, INRS-Energie, CANADA
Dr. R. Bolton, Centre canadien de fusion magnétique, CANADA
Dr. C.R. James,, Univ. of Alberta, CANADA
Dr. P. Lukác, Komenského Universzita, CZECHO-SLOVAKIA
The Librarian, Culham Laboratory, ENGLAND
Library, R61, Rutherford Appleton Laboratory, ENGLAND
Mrs. S.A. Hutchinson, JET Library, ENGLAND
Dr. S.C. Sharma, Univ. of South Pacific, FIJI ISLANDS
P. Mähönen, Univ. of Helsinki, FINLAND
Prof. M.N. Bussac, Ecole Polytechnique,, FRANCE
C. Mouttet, Lab. de Physique des Milieux Ionisés, FRANCE
J. Radet, CEN/CADARACHE - Bat 506, FRANCE
Prof. E. Economou, Univ. of Crete, GREECE
Ms. C. Rinni, Univ. of Ioannina, GREECE
Dr. T. Mual, Academy Bibliographic Ser., HONG KONG
Preprint Library, Hungarian Academy of Sci., HUNGARY
Dr. B. DasGupta, Saha Inst. of Nuclear Physics, INDIA
Dr. P. Kaw, Inst. for Plasma Research, INDIA
Dr. P. Rosenau, Israel Inst. of Technology, ISRAEL
Librarian, International Center for Theo Physics, ITALY
Miss C. De Palo, Associazione EURATOM-ENEA , ITALY
Dr. G. Grosso, Istituto di Fisica del Plasma, ITALY
Prof. G. Rostangni, Istituto Gas Ionizzati Del Cnr, ITALY
Dr. H. Yamato, Toshiba Res & Devel Center, JAPAN
Prof. I. Kawakami, Hiroshima Univ., JAPAN
Prof. K. Nishikawa, Hiroshima Univ., JAPAN
Director, Japan Atomic Energy Research Inst., JAPAN
Prof. S. Itoh, Kyushu Univ., JAPAN
Research Info. Ctr., National Instit. for Fusion Science, JAPAN
Prof. S. Tanaka, Kyoto Univ., JAPAN
Library, Kyoto Univ., JAPAN
Prof. N. Inoue, Univ. of Tokyo, JAPAN
Secretary, Plasma Section, Electrotechnical Lab., JAPAN
S. Mori, Technical Advisor, JAERI, JAPAN
Dr. O. Mitarai, Kumamoto Inst. of Technology, JAPAN
J. Hyeon-Sook, Korea Atomic Energy Research Inst., KOREA
D.I. Choi, The Korea Adv. Inst. of Sci. & Tech., KOREA
Prof. B.S. Liley, Univ. of Waikato, NEW ZEALAND
Inst of Physics, Chinese Acad Sci PEOPLE'S REP. OF CHINA
Library, Inst. of Plasma Physics, PEOPLE'S REP. OF CHINA
Tsinghua Univ. Library, PEOPLE'S REPUBLIC OF CHINA
Z. Li, S.W. Inst Physics, PEOPLE'S REPUBLIC OF CHINA
Prof. J.A.C. Cabral, Instituto Superior Tecnico, PORTUGAL
Dr. O. Petrus, AL I CUZA Univ., ROMANIA
Dr. J. de Villiers, Fusion Studies, AEC, S. AFRICA
Prof. M.A. Hellberg, Univ. of Natal, S. AFRICA
Prof. D.E. Kim, Pohang Inst. of Sci. & Tech., SO. KOREA
Prof. C.I.E.M.A.T, Fusion Division Library, SPAIN
Dr. L. Stenflo, Univ. of UMEA, SWEDEN
Library, Royal Inst. of Technology, SWEDEN
Prof. H. Wilhelmson, Chalmers Univ. of Tech., SWEDEN
Centre Phys. Des Plasmas, Ecole Polytech, SWITZERLAND
Bibliotheek, Inst. Voor Plasma-Fysica, THE NETHERLANDS
Asst. Prof. Dr. S. Cakir, Middle East Tech. Univ., TURKEY
Dr. V.A. Glukhikh,Sci. Res. Inst. Electrophys.I Apparatus, USSR
Dr. D.D. Ryutov, Siberian Branch of Academy of Sci., USSR
Dr. G.A. Eliseev, I.V. Kurchatov Inst., USSR
Librarian, The Ukr.SSR Academy of Sciences, USSR
Dr. L.M. Kovrizhnykh, Inst. of General Physics, USSR
Kernforschungsanlage GmbH, Zentralbibliothek, W. GERMANY
Bibliothek, Inst. Für Plasmaforschung, W. GERMANY
Prof. K. Schindler, Ruhr-Universität Bochum, W. GERMANY
Dr. F. Wagner, (ASDEX), Max-Planck-Institut, W. GERMANY
Librarian, Max-Planck-Institut, W. GERMANY
Prof. R.K. Janev, Inst. of Physics, YUGOSLAVIA

END

DATE
FILMED
6/17/92